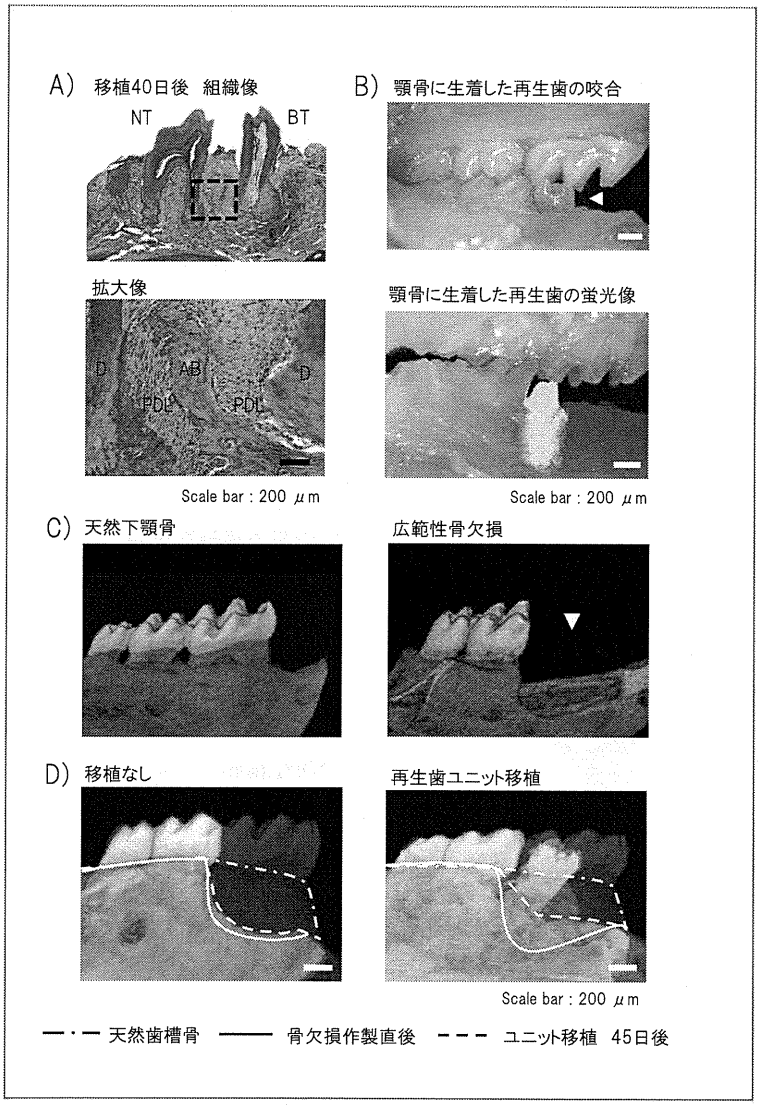

図10 再生歯ユニットの生着と歯槽骨回復効果

A) 移植40日後の顎骨に生着した再生歯ユニットの組織像。NT：天然歯，BT：再生歯，D：象牙質，AB：歯槽骨，PDL：歯根膜。

B) 顎骨に骨性結合をした再生歯ユニット（上図）と蛍光色素を沈着させた再生歯の蛍光画像（下図）。

C) 成体マウスの天然下顎骨（左図）と，広範性骨欠損モデル（右図，矢頭：欠損部）。

D) 広範性骨欠損モデルに再生歯を移植して45日後のCT像の重ね合わせ。正常な歯槽骨レベル（一点鎖線：一・一），広範性骨欠損モデル作成時の骨レベル（実線：———），再生歯ユニットの非移植群，移植群の骨の回復レベル（点線：- - - -）。

3）再生歯の機械的外力への応答

歯根膜は，過剰な機械的外力に対する緩衝能を有するばかりでなく，歯科矯正治療における歯槽骨のリモデリングを介した歯の移動において重要な役割を果たすことが知られている（図11 - A）。そこで，再生歯胚移植によって萌出した再生歯に実験的矯正を加えると矯正６日目には歯周囲の歯根膜の形態が変化すると共に，牽引側では骨形成が起こり，逆に圧迫側では骨吸収が認められ，矯正17日目には再生歯が天然歯と同様に移動することが判明した（図11 - B）。また，再生歯ユニット移植によって生着した再生歯によっても同様の結果が認められた。

これらのことから，再生歯は顎顔面領域の連携機能を修復することにより，歯根膜を介した歯の生理的機能を再生することが示された[7,13]。

4）再生歯の知覚神経機能

末梢神経系は，胎児期において発生している器官からの誘引と中枢神経との連結によって確立され，臓器機能の発現制御や侵害刺激の中枢への伝達に重要な役割を果たすことが知られている。歯には知覚性の三叉神経が侵入しており，歯の正常な機能発現と保護に重要であることから，知覚性の神経機能を回復させる歯科再生治療が期待されている。

最近，私たちは再生歯胚を移植することにより，萌出した再生歯の歯髄と歯根膜に交感神経や知覚神経などの神経線維が侵入していることを明らかにすると共に（図12），それらが正常に侵害刺激を受容して中枢神経系に伝達することを実証した[7]。さらに完成歯である再生歯ユニット移植においても

同様に，神経線維の侵入，ならびに中枢神経系への刺激伝達が可能であることを明らかにした[13]。

これらの結果から，再生歯による歯全体の再生治療は，咀嚼や機械的外力に対する応答だけではなく，侵害刺激を中枢に伝達するという歯の機能も再生できる可能性が示された[7,13]。

6．結び

この数年間の間に，歯科再生医療の技術開発は大きな進展を見せ，組織修復療法のみならず，歯をまるごと再生するための治療法として再生歯胚の移植治療や再生歯ユニットを用いた歯周組織を含めた包括的な治療法の概念が示された。今後，これらの治療法を実用化するには未だ解決すべき課題が残されている。

組織修復療法は，治療に必要な幹細胞はほぼ特定されており，患者本人の細胞を利用した臨床研究が進められている。またヒトサイトカインもその作用機序も明らかにされつつあり，今後，再生治療用医薬品としての臨床開発が加速されることが期待される。一方，歯をまるごと再生する治療の実現には，免疫学的な拒絶反応を避けるため，患者に由来する細胞を用いて歯胚を再生する必要がある。この細胞シーズの探索研究は，現在，世界中で進められており，組織修復のための組織幹細胞では歯胚再生の細胞シーズとしては不十分であり，胎児期の歯胚誘導を再現しうる能力をもつ幹細胞や，多能性のiPS細胞からの歯胚誘導などの研究開発が期待される。

また，歯をまるごと再生するための治療法としては，ヒトの場合には再生歯胚から歯を再生するには数年の期間が必要であるため，再生歯ユニットを移植する治療技術の開発が期待される。そのためには，再生歯胚を生体外で培養し，短期間で移植可能な再生歯を製造する技術開発も必要である。現在のところ，細胞凝集塊や組織，器官を培養可能なシステムの開発は十分ではなく，三次元的な培養システムや，それを三次元的な血管ネットワークシステムを利用した培養システムの開発などに連携させることにより，その実現が図れるものと考えられる。

今後，歯科再生治療に向けた基盤技術開発と臨床応用化研究を推進することによって，歯科再生治療を実現することが期待されると共に，歯科再生治療が臓器置換再

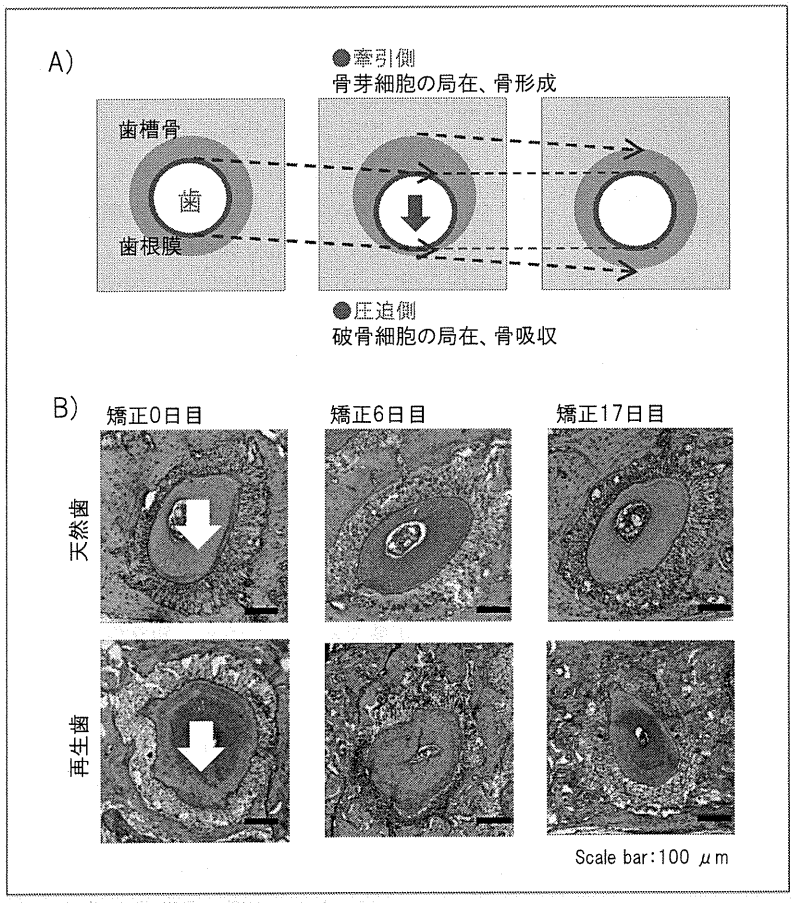

図11　再生歯歯根膜の骨リモデリング能
A）矯正力を加えた場合の歯の移動の模式図。
B）天然歯（上段）ならびに再生歯（下段）における矯正0日目，6日目，17日目の組織像。

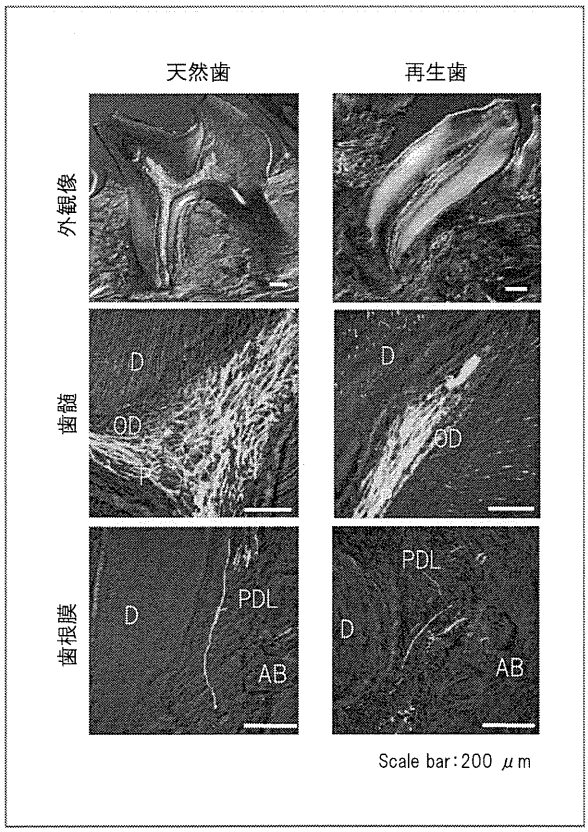

図12　再生歯の神経機能
天然歯および再生歯の歯髄ならびに歯根膜の神経線維の分布。D：象牙質，OD：象牙芽細胞，P：歯髄，AB：歯槽骨，PDL：歯根膜。

生医療の最先端のフィージビリティスタディモデルとして，幅広い臓器・器官再生研究に応用されることが期待される[1,5]。

＜謝辞＞
本研究は，厚生労働省科学研究費補助金・再生医療実用化研究事業（H21～23年度，代表：東京医科歯科大学・山口朗教授），文部科学省・特定領域研究「マルチスケール操作によるシステム細胞工学」（H17～21年度，代表：名古屋大学・福田敏男教授），文部科学省・科学研究費補助金・基盤研究A（H20～22年度，代表：辻　孝），同・若手研究B（H22～23年度，代表：大島正充），株式会社オーガンテクノロジーズ共同研究費などの研究費により行われました。

参考文献

1) Ikeda, E. and Tsuji, T.: Growing bioengineered teeth from single cells: potential for dental regenerative medicine. Expert Opin. Biol. Ther., 8 : 735～744, 2008.
2) Pispa, J. and Thesleff, I.: Mechanisms of ectodermal organogenesis. Dev. Biol., 262 : 195～205, 2003.
3) Brenemark PI, Zarb, G. A., Albrektsson, T.: Osseointegration in clinical dentistry. Quintessence, 1985.
4) Gurtner, G. C., Werner, S., Barrandon, Y. and Longaker, M. T.: Wound repair and regeneration. Nature, 453 : 314～321, 2008.
5) Sharpe, P. T. and Young, C. S.: Test-tube teeth. Sci. Am., 293 : 34～41, 2005.
6) Nakao, K. et al.: The development of a bioengineered organ germ method. Nat. Methods., 4 : 227～230, 2007.
7) Ikeda, E. et al.: Fully functional bioengineered tooth replacement as an organ replacement therapy. Proc. Natl. Acad. Sci. USA., 106 : 13475～13480, 2009.
8) Gronthos, S., Mankani, M., Brahim, J., Robey, P. G. and Shi, S.: Postnatal human dental pulp stem cells (DPSCs) in vitro and in vivo. Proc. Natl. Acad. Sci. USA., 97 : 13625～13630, 2000.
9) Miura, M. et al.: SHED: stem cells from human exfoliated deciduous teeth. Proc. Natl. Acad. Sci. USA., 100 : 5807～5812, 2003.
10) Sonoyama, W. et al.: Mesenchymal stem cell-mediated functional tooth regeneration in swine. PLoS ONE, 1 : e79, 2006.
11) Seo, B. M. et al.: Investigation of multipotent postnatal stem cells from human periodontal ligament. Lancet, 364 : 149～155, 2004.
12) Ishida, K. et al.: The regulation of tooth morphogenesis is associated with epithelial cell proliferation and the expression of sonic hedgehog through epithelial-mesenchymal interactions. Biochem. Biophys. Res. Commun., 405 : 455～461, 2011.
13) Oshima, M. et al.: Functional tooth regeneration using a bioengineered tooth unit as a mature organ replacement regenerative therapy. PLoS ONE, 6 (7) : e21531, 2011.

Ⅱ. 歯

2. 歯周病と炎症

Periodontitis and inflammation

松下 健二
Kenji Matsushita(部長)／国立長寿医療研究センター口腔疾患研究部

key words

Porphyromonas gingivalis
gingipain
HMGB1
血管炎症
E-selectin

歯周病の病態形成には，細菌感染による炎症反応と非感染性の慢性炎症が複雑に絡み合っている．歯周ポケットに存在する各種の歯周病関連細菌は，Toll 様受容体を活性化し，歯周組織の慢性炎症形成に寄与している．加えて，HMGB1などの内因性リガンドが恒常的な炎症反応を誘導する．また，歯周病関連細菌 *P. gingivalis* は血管内皮との相互作用により，血管炎症を進展させる．

歯周病は細菌感染を伴った慢性炎症性疾患である

歯周病は感染症であり，歯周病関連細菌によって惹起される炎症性疾患である．また，その発症と進行にはそれらの細菌の病原性だけではなく，歯周組織における宿主側の各種細胞の応答が深く関与する[1]．歯周ポケットには，グラム陰性桿菌をはじめとした数多くの細菌が生息し，競合・共生関係を維持しながら細菌叢を形成している．そのなかで，特定の細菌が歯周病の発症や進行に関与しており，特に関連性が高いと考えている細菌として，*Porphyromonas gingivalis, Actinobacillus actinomycetemcomitans, Tannerella forsythia, Treponema Denticola* などが知られている[2]．それらの菌は，内毒素，蛋白分解酵素，線毛などの病原因子を有しており，それらの菌が歯周組織に感染する際の重要な因子となる．また，同因子は歯周組織において宿主細胞を活性化し，強力に炎症反応および免疫応答を惹起する．歯周ポケットに形成される細菌叢は時にグリコカリックス様の構造物で被覆され，バイオフィルムの形態を呈する．このようなバイオフィルムを形成した歯周病関連細菌は，抗体，食細胞，抗生物質に対して抵抗性を示すことから，歯周組織に細菌が持続感染しやすい状態となる[3]．このような細菌と宿主の相互作用が持続することと，さまざまな環境因子や遺伝因子が複雑に絡み合って，歯周病の慢性炎症病態が形成されるものと考えられる(図1)．

生活習慣病は慢性炎症性疾患である

近年，肥満，糖尿病，動脈硬化性疾患などの生活習慣病，アルツハイマー病，パーキンソン病などの神経変性疾患，関節リウマチなどの自己免疫疾患，癌などに共通する分子基盤として慢性炎症が注目されている．慢性炎症では長期にわたるストレス応答によって炎症反応が遷延化するとともに，宿主の恒常性が十分維持されず破綻をきたし，不可逆的な組織のリモデリングを生じ，組織・臓器の機能不全をきたすようになる[4]．たとえば，動脈硬化では血管壁に対して，物理的，科学的刺激により内皮細胞や血管平滑筋細胞の機能が変化する．この内皮細胞の機能障害は脂質などの血管壁への浸透・蓄積，血

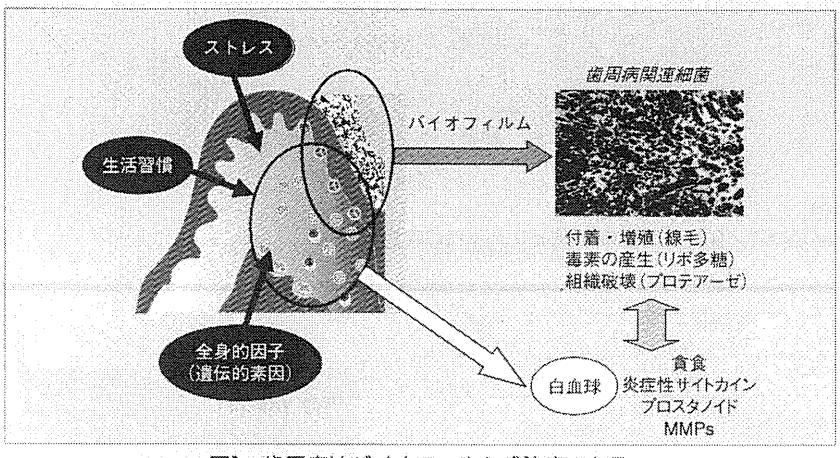

図1　歯周病はバイオフィルム感染症である

歯周病においては，歯周ポケットに生息する細菌群が歯周組織を直接傷害するとともに，各種菌体毒素によって宿主細胞を活性化し，炎症反応が惹起される．加えて，それらの細菌はバイオフィルムを形成し，宿主あるいは抗菌薬に対して抵抗性を示す．

管内皮への白血球の浸潤を引き起こす．このような細胞応答が長期に持続することにより，血管壁の破壊とそれに伴う修復反応が同時に進行し，その結果，組織構築が改変されることになる[5]．以上のような，複雑な細胞・組織応答が他の慢性炎症性疾患にも共通して認められる現象である．近年，歯周病と動脈硬化性疾患や糖尿病などの生活習慣病との関連性が注目されているが，両者の間には単に相関関係が認められるというだけではなく，その発症機序に共通の分子基盤が存在していることが考えられる．歯周病を生活習慣病として捉え，生活習慣病の共通分子基盤である慢性炎症といった視点から考えることは，両者の関係をより深く理解するために極めて重要である．

慢性炎症には臓器特異性が認められる一方，臓器を超えた共通の分子機構が存在する可能性が高い．慢性炎症は，微生物感染により誘導されるものと感染が関連しないものとに大別される．歯周病は前者に属し，糖尿病や動脈硬化性疾患などはおおむね後者に属するものと考えられる．ただし，歯周病の病態形成には細菌感染による炎症反応と非感染性の慢性炎症が複雑に絡み合っているものと考えられる[8]（図2）．

自然炎症としての歯周病

感染症における免疫反応の機序における重要な分子として，Toll 様受容体（Toll-like receptor ： TLR）をはじめとする病原体センサーが重要な役割を担うことが知られている．免疫システムにおいて，病原体などの外来抗原をいかに認識するかは極めて重要であり，TLR はそれらを認識し，自然免疫応答を誘導して炎症反応を惹起する重要な分子である[9]．歯周ポケットに存在する各種の歯周病関連細菌は，これらの受容体を活性化し，歯周組織の慢性炎症形成に寄与しているものと考えられる．歯周病関連細菌の一種である *P.gingivalis* はこれらのリガンドを数多く有し，樹状細胞やマクロファージなどを活性化し，自然免疫応答とともに炎症反応を強力に惹起する．*P.gingivalis* のリポ多糖（LPS）は，他のグラム陰性菌のそれとは異なり，細胞壁のリポ蛋白，リポタイコ酸やペプチドグリカンと同様に TLR2のリガンドとなり得ることも報告されている．そして，同受容体の活性化を介して，マクロファージや単球の活性化に寄与する．また，同菌の菌体表層に存在する線毛は歯周局所への付着・定着に関与するだけでなく，同受容体を介して，炎症性サイトカイン産生を誘導することも報告されている[8][9]．TLR からのシグナルは，MyD88などのシグナル伝達物質を介して，NF-κB（nuclear factor-κB）や IRF（interferon regulatory factor）などの転写因子を活性化し，TNF-α や IL-6（interlenkin-6）といった炎症性サイトカインの産生を誘導する[10]．また，同菌の産生するシステインプロテアーゼ gingipain は，間質のマトリックス蛋白質を分解し，歯周組織を直接破壊するだけでなく，好中球受容体や補体を分解し宿主の免疫反応を抑制する．他方で，マトリックスメタロプロテアーゼ（MMP）や炎症性サイトカインの産生を誘導し，炎症反応を促進する（図3）．さらに，血液凝固因子である Factor X や プロトロンビンなどを活性化し，血液凝固反応

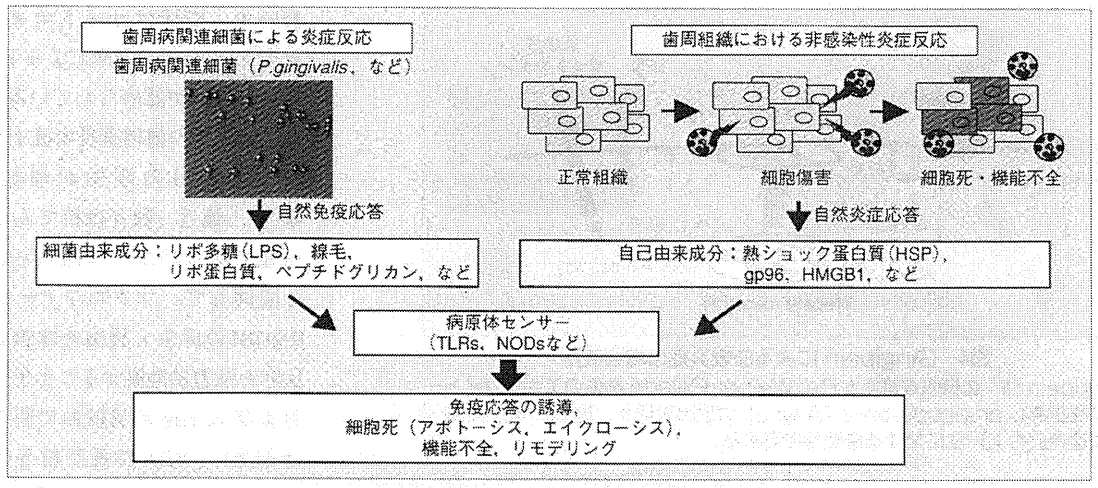

図2　慢性炎症としての歯周病の発症機序

歯周病関連細菌の毒素は，宿主の病原センサーに補足され，宿主細胞の免疫応答を促す．加えて，傷害を受けた細胞は細胞から放出される自己由来成分も同受容体を介して炎症反応を惹起する．これらが複合して慢性炎症としての歯周病の病態が形成される．NOD：nucleotide oligomerization domain

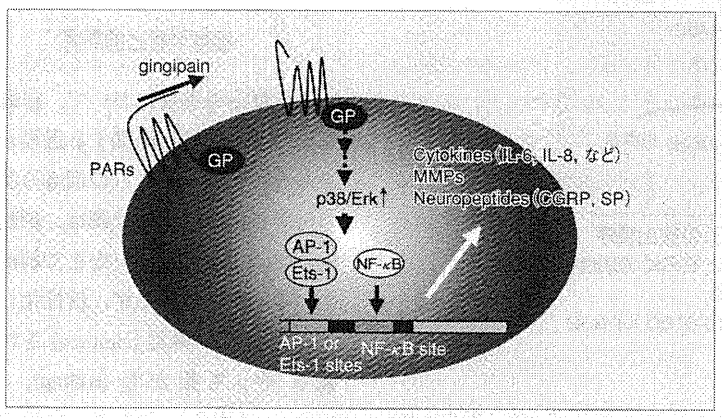

図3　Gingipainが炎症反応を惹起する仕組み

P.gingivalis が産生するトリプシン様システインプロテアーゼgingipainは，PARの活性化を介して，サイトカイン，マトリックスメタロプロテアーゼ，神経ペプチドなどの発現を誘導して炎症反応を惹起する．

を誘導したりもする[11]．我々は，gingipainが血管内皮細胞に発現するPAR（protease-activated receptor）を活性化し，同細胞における血管形成調節因子angiopoietin 2を含む分泌顆粒のエキソサイトーシスを誘導し，LPSに対する感受性を高めて血管の炎症応答を亢進することを明らかにした[12]（図4）．このように，歯周病関連細菌は歯周組織に侵入・定着し，さまざまな病原因子を産生して，歯周組織の炎症反応を惹起している．加えて，組織障害に伴って放出される内因性リガンドがTLRなどの病原体センサーを活性化し，外因性リガンドの刺激と相まって感染症における慢性炎症の病態形成に寄与していることが考えられている．傷害を受けたり，壊死したりした細胞はそこに潜む危険を排除するために，免疫系の細胞の活性化を促すようなシグナル（danger signal）を発し，炎症反応を引き起こすことが知られている．このような分子は，DAMPs（danger-associated molecular patterns）とも呼ばれ，ATP，尿酸結晶，HSP（heat shock protein），HMGB1（high mobility group box protein-1）などが知られている．DAMPsは，宿主が自分自身を守り自らを再生させるために生ずると考えられるが，一方こうした

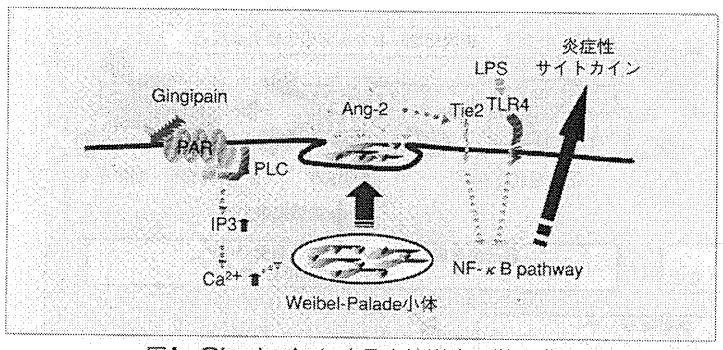

図4　Gingipainによる血管炎症の増強機序
gingipainは，血管内皮細胞からのWeibel-Palade小体のエキソサイトーシスを誘導しangiopoietin-2（Ang-2）の放出を促す．放出されたAng-2は血管内皮のLPSに対する感受性を高める．

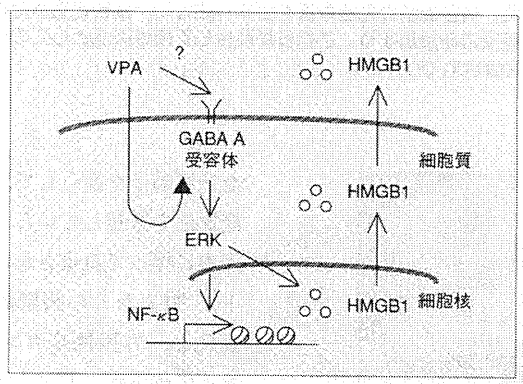

図5　バルプロ酸によるHMGB1の放出機序
バルプロ酸（VPA）はGABA受容体とERKの活性化を介して，HMGB1の放出を誘導する．
ERK：extracellular signal-regulated kinase

免疫応答が過剰に働き，炎症反応が必要以上に生ずるとさまざまな慢性疾患の発症や進行へとつながってゆく[13]．そのような分子の一つであるHMGB1は，細胞核に存在するDNA結合蛋白質の一種で遺伝子の転写を制御する因子である．HMGB1の受容体として，RAGE（receptor for advanced glycation end products），TLR2/4などが知られている[14]．同分子は細胞死によって細胞から漏出するが，活性化した単核球からもHMGB1は放出され炎症反応を惹起することが知られており，多くの炎症性疾患へのHMGB1の関与が示されている．具体的には敗血症の致死因子として，あるいは腎炎，肝炎，肺炎などの慢性炎症病態の形成に関与する因子として注目されている．歯周病との関与もいくつか報告されている．歯肉上皮細胞や歯肉由来線維芽細胞において，炎症性サイトカインTNF-αやLPSなどの刺激によるHMGB1の産生・放出が認められている[15]．また，慢性歯周炎の歯肉溝浸出液中や歯肉上皮にHMGB1の産生が増加している[16][17]．最近，我々は抗てんかん薬の一種であるバルプロ酸（VPA）がLPSと協同して，マクロファージからのHMGB1の産生・放出を増強し，炎症反応を強力に進展することを，*in vitro*および*in vivo*の実験系で明らかにした（図5）．VPAの長期投与の副作用として，歯肉増殖症と歯周炎の増悪が知られているが，VPAは歯周組織の炎症の増悪因子である可能性が示唆された．

血管炎症と歯周病

炎症反応の進展において，白血球が血管内から組織へ浸潤する過程が重要である．また，それらの細胞の血管への付着と血管外への浸潤は，細胞接着因子およびモノカインなどで制御されている．白血球はまず，活性化した血管内皮細胞に補足（capture）され，血管にそって転がり（rolling），付着（adhesion）する．その後，血管内皮細胞を通り抜け血管外へと移動し，組織へ浸潤する．特に，captureからrollingの過程で重要になってくる分子がselectinである[18]．血管内皮細胞には，E-selectinという同細胞に特異的に発現しているselectinが存在し白血球と同細胞との相互作用に寄与している．E-selectinは，TNF-α，IL-1β，LPSなどにより活性化した血管内皮細

胞に発現する．E-selectin は白血球上のリガンドである sialyl lewis X と相互作用し，白血球の rolling を誘発する．また，E-selectin の一部は，細胞外領域で切断され可溶性 E-selectin (sE-selectin) として血中に遊離される．敗血症や膠原病などの炎症性疾患，血栓性血小板減少性紫斑病のような微小血管障害および冠動脈疾患，脳血管障害，閉塞性末梢動脈疾患などの動脈硬化性疾患の患者において血中 sE-selectin 濃度が高値を示すことが知られている．重度の歯肉炎患者の血漿中あるいは歯肉溝浸出液中にも高濃度の sE-selectin が検出される．近年，閉塞性血栓性血管炎と歯周病との関連性が報告され，血管病変部に歯周病関連細菌が高頻度に検出されることが示されている．我々は，歯周病関連細菌，特に *P.gingivalis* が血管病変部に定着する機序の一つとして E-selectin に着目し，同分子と *P.gingivalis* との相互作用について検討した．その結果，TNF-α で刺激した血管内皮細胞上では，*P.gingivalis* の付着が著しく亢進すること，またそれは E-selectin 抗体および sialyl lewis X の添加によって有意に抑制されることを明らかにした (図6)．また従来，血管内皮への *P.gingivalis* の付着には，同菌の線毛が重要であることが報告されてきたが，E-selectin との相互作用には OmpA 様外膜蛋白質が重要であることが明らかになった．これらの結果は，炎症血管においては，*P.gingivalis* が付着しやすいこと，またその付着様式は上皮や正常血管内皮とのそれと異なる可能性が考えられた．このように血管炎症部位に付着した *P.gingivalis* は，その後，細胞あるいは組織に侵入し持続感染を成立させるとともに，血管炎症を増強する可能性が考えられる (図7)．

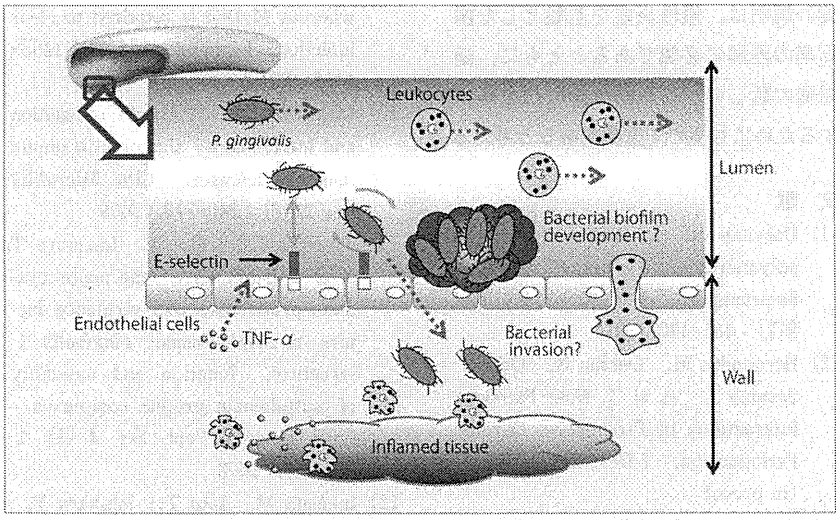

図6　E-selectin を介した *P.gingivalis* の血管付着
P.gingivalis は，E-selectin を介して活性化した血管内皮と付着する．その後，同菌は血管内皮に侵入，あるいは内皮上にバイオフィルムを形成し，血管炎症を増強する可能性がある．

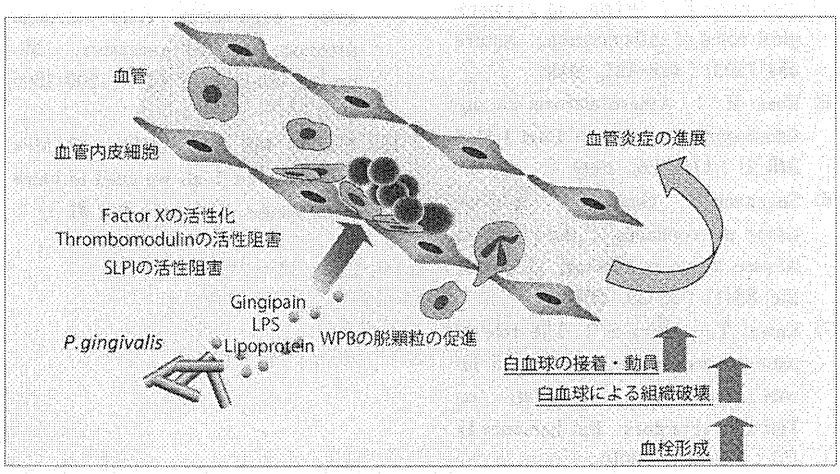

図7　*P.gingivalis* が血管炎症を増悪する機序
P.gingivalis が産生する種々の毒素は，白血球の活性化および血管内皮への接着・動員とそれによる血管傷害，さらには血管内における血栓形成を促進し，血管炎症を進展させる可能性がある．

歯周病関連細菌の血管炎症への関与は，歯周病の病態形成に極めて重要である．その分子機構と病態生理学的意

養の解明は，慢性炎症を基盤とした歯周病の理解に必須であるとともに，歯周病の新しい治療戦略や診断法を確立するためにも極めて重要であると考える．

文 献

1) Darveau RP：Periodontitis；a polymicrobial disruption of host homeostasis. Nat Rev Microbiol **8**(7)：481-490, 2010
2) Hernandez M, Dutzan N, Garcia-Sesnich J, et al：Host-Pathogen Interactions in Progressive Chronic Periodontitis. J Dent Res, 2011, (in press)
3) Berezow AB, Darveau RP：Microbial shift and periodontitis. Periodontol 2000 **55**(1)：36-47, 2010
4) Medzhitov R：Origin and physiological roles of inflammation. Nature **454**(7203)：428-435, 2008
5) Ross R：Atherosclerosis-an inflammatory disease. N Engl J Med **340**(2)：115-126, 1999
6) Suganami T, Ogawa Y：Adipose tissue macrophages；their role in adipose tissue remodeling. J Leukoc Biol **88**(1)：33-39, 2010
7) Kawai T, Akira S：The role of pattern-recognition receptors in innate immunity；update on Toll-like receptors. Nat Immunol **11**(5)：373-384, 2010
8) Zhang P, Liu J, Xu Q, et al：TLR2-dependent Modulation of Osteoclastogenesis by *Porphyromonas gingivalis* through Differential Induction of NFATc1 and NF-κB. J Biol Chem **286**(27)：24159-24169, 2011
9) Burns E, Eliyahu T, Uematsu S, et al：TLR2-dependent inflammatory response to *Porphyromonas gingivalis* is MyD88 independent, whereas MyD88 is required to clear infection. J Immunol **184**(3)：1455-1462, 2010
10) Mogensen TH：Pathogen recognition and inflammatory signaling in innate immune defenses. Clin Microbiol Rev 22(2)：240-273, 2009
11) Potempa J, Sroka A, Imamura T, et al：Gingipains, the major cysteine proteinases and virulence factors of *Porphyromonas gingivalis*；structure, function and assembly of multidomain protein complexes. Curr Protein Pept Sci **4**(6)：397-407, 2003
12) Inomata M, Into T, Ishihara Y, et al：Arginine-specific gingipain A from *Porphyromonas gingivalis* induces Weibel-Palade body exocytosis and enhanced activation of vascular endothelial cells through protease-activated receptors. Microbes Infect **9**(12-13)：1500-1506, 2007
13) Bianchi ME：DAMPs, PAMPs and alarmins；all we need to know about danger. J Leukoc Biol **81**(1)：1-5, 2007
14) Huang W, Tang Y, Li L：HMGB1, a potent proinflammatory cytokine in sepsis. Cytokine **51**(2)：119-126, 2010
15) Morimoto Y, Kawahara KI, Tancharoen S, et al：Tumor necrosis factor-alpha stimulates gingival epithelial cells to release high mobility-group box 1. J Periodontal Res **43**(1)：76-83, 2008
16) Luo L, Xie P, Gong P, et al：Expression of HMGB1 and HMGN2 in gingival tissues, GCF and PICF of periodontitis patients and peri-implantitis. Arch Oral Biol 2011(in press)
17) Ebe N, Hara-Yokoyama M, Iwasaki K, et al：Pocket epithelium in the pathological setting for HMGB1 release. J Dent Res **90**(2)：235-240, 2011
18) Kneuer C, Ehrhardt C, Radomski MW, et al：Selectins--potential pharmacological targets? Drug Discov Today **11**(21-22)：1034-1040, 2006

松下 健二（Kenji Matsushita）
鹿児島大学歯学部卒業，同大学博士課程を終え，1993年より同学部歯科保存学講座（1）助手，2002年より米国ジョンス・ホプキンス大学医学部循環器内科において血管炎症の制御に関する研究に従事．2005年に帰国し，国立長寿医療研究センター口腔疾患研究部部長，現在に至る．

SHOCK, Vol. 36, No. 5, pp. 494–500, 2011

VALPROIC ACID INCREASES SUSCEPTIBILITY TO ENDOTOXIN SHOCK THROUGH ENHANCED RELEASE OF HIGH-MOBILITY GROUP BOX 1

Shinsuke Sugiura,*† Yuichi Ishihara,† Toshinori Komatsu,* Makoto Hagiwara,* Naomi Tanigawa,* Yoshiko Kato,*† Hiroki Mizutani,† Ko-ichi Kawahara,‡ Ikuro Maruyama,‡ Toshihide Noguchi,† and Kenji Matsushita*†

**Department of Oral Disease Research, National Center for Geriatrics and Gerontology, Obu; †Department of Periodontology, School of Dentistry, Aichi Gakuin University, Nagoya, Aichi; and ‡Department of Laboratory and Molecular Medicine, Shin Nippon Biomedical Laboratories Inc, Kagoshima University, Kagoshima, Japan*

Received 17 Mar 2011; first review completed 1 Apr 2011; accepted in final form 21 Jul 2011

ABSTRACT—High-mobility group box 1 (HMGB1) is a nuclear factor and a secreted protein. During inflammation, HMGB1 is secreted into the extracellular space where it can interact with the receptor for advanced glycation end products and trigger proinflammatory signals. Extracellular HMGB1 plays a critical role in several inflammatory diseases such as sepsis and rheumatoid arthritis. Valproic acid (VPA) is one of the most frequently prescribed antiepileptic drugs. The present study was undertaken to investigate the effect of VPA on secretion of HMGB1 in systemic inflammatory responses induced by lipopolysaccharide. Pretreatment with VPA increased the susceptibility of mice to lipopolysaccharide in endotoxemia. Valproic acid induced HMGB1 release and nuclear factor κB activation in RAW-blue cells. Valproic acid promoted the phosphorylation of ERK1/2 but not that of p38 or JNK. The MEK1/2 inhibitor PD98059 also suppressed HMGB1 release and activation of nuclear factor κB induced by VPA. Valproic acid induced expression of γ-aminobutyric acid receptors in macrophages, and picrotoxin, a γ-aminobutyric acid A receptor antagonist, inhibited the VPA-activated phosphorylation of ERK and VPA-induced HMGB1 release. These results suggest that VPA may exacerbate innate immune responses to endotoxin through enhanced release of HMGB1.

KEYWORDS—Sepsis, alarmin, lipopolysaccharide, histone deacetylases, inflammation, immunomodulation, cytokines

INTRODUCTION

Sequential cytokine induction by cells of the mononuclear phagocyte system has been found *in vitro* and *in vivo* following endotoxin stimulation. These cytokines, such as tumor necrosis factor (TNF), interleukin 6 (IL-6) and IL-1, are thought to be important as regulators of the immune system under physiologic conditions. However, excessive amounts of cytokines play a role in the pathologic manifestations of endotoxemia. High-mobility group box 1 (HMGB1), a protein previously known as a nuclear transcription factor, is a critical mediator of lethality in endotoxemia and sepsis (1). During a systemic inflammatory response, HMGB1 is released into the circulation by activated monocytes and by damaged cells. Administration of antibodies to HMGB1 attenuates endotoxin lethality in mice. Therefore, it is thought that HMGB1 is an important mediator of lethal systemic inflammation (1).

Inhibitors of nuclear histone deacetylases (HDACs) have been shown to suppress cancer cell proliferation *in vitro* (2, 3) and reduce experimental tumor growth *in vivo* (4, 5). Histone deacetylase inhibitors include short-chain fatty acids, hydroxamic acids, cyclic tetrapeptides, and benzamides. Suberoylanilide hydroxamid acid (SAHA)—the classic member of the class of hydroxamic acids—has potent anti-inflammatory activities, both *in vitro* and *in vivo* (6, 7). Histone deacetylase inhibition was shown to be associated with significant suppression of the production of proinflammatory cytokines (8, 9). These anti-inflammatory properties were confirmed by studies demonstrating that treatment with SAHA resulted in a significant reduction of disease severity in a murine model of systemic lupus erythematosus, the MLR-*lpr/lpr* mouse (10). The anti-inflammatory effects described for HDAC inhibitors have so far been limited to SAHA (11) and trichostatin A (TSA) (8, 12), both members of the class of hydroxamic acids. Thus, it remains to be clarified whether the anti-inflammatory effects of HDAC inhibition are restricted to this class or whether inhibition of HDACs in general results in suppression of cytokine production.

Many studies show that various HDAC inhibitors suppress inflammation. A few studies show that select HDAC inhibitors can increase inflammation. The differences between these results are probably explained by differences in the specificity of HDAC inhibitors and the various animal models used to uncover the mechanisms of inflammation.

Valproic acid (VPA) is an HDAC inhibitor of the class of short-chain fatty acids (13), and it is an established drug in the treatment of epileptic seizures and bipolar disorder (14). Accumulated experimental and clinical data also show that VPA might be a potent anticancer drug (15). Valproic acid also has anti-inflammatory effects (16). On the other hand, in some cases, VPA augments inflammatory responses: patients

Address reprint requests to Kenji Matsushita, DDS, PhD, Department of Oral Disease Research, National Center for Geriatrics and Gerontology, Obu, Aichi 4747-8511, Japan. E-mail: kmatsu30@ncgg.go.jp.

This work was supported by Grants-in-Aid for Scientific Research 22390354 and 21659436 (to K.M.) from the Ministry of Education, Culture, Sports, Science and Technology, Japan.

Supplemental digital content is available for this article. Direct URL citation appears in the printed text and is provided in the HTML and PDF versions of this article on the journal's Web site (www.shockjournal.com).

DOI: 10.1097/SHK.0b013e31822f7e58

receiving VPA may well develop hemorrhagic pancreatitis, bone marrow suppression, and hepatotoxicity (17, 18). Gingival overgrowth and progression of gingival inflammation are sometimes observed in patients who are taking VPA chronically (19). However, the mechanisms underlying the inflammatory effects of VPA are not known. In the present study, we found that VPA enhanced systemic inflammatory responses induced by lipopolysaccharide (LPS) by promoting the secretion of HMGB1 in murine macrophage cultures and in a murine model of endotoxic shock.

MATERIALS AND METHODS

Materials

Valproic acid and SAHA were purchased from Sigma-Aldrich (St Louis, Mo). Trichostatin A was purchased from Calbiochem (San Diego, Calif). *Escherichia coli* O18 LPS and TNF-α were purchased from Sigma-Aldrich. Purified rabbit polyclonal antibodies to HMGB1 and chicken polyclonal antibodies to HMGB1 were purchased from SHINO-TEST (Tokyo, Japan). Mouse monoclonal antibodies to phospho-ERK1/2, p38, and JNK were purchased from Cell Signaling Technology (Beverly, Mass). Mouse monoclonal antibodies to ERK1/2, p38, and JNK were purchased from BD Bioscience (Franklin Lakes, NJ). Mouse monoclonal antibodies to β-actin were purchased from BioVision (San Francisco, Calif).

Cell culture

RAW-blue cells were established from RAW 264.7 macrophage cells (InvivoGen, San Diego, Calif). They stably express a secreted embryonic alkaline phosphatase gene inducible by nuclear factor κB (NF-κB) and AP-1 transcription factors. RAW-blue cells were precultured in RPMI 1640 medium (Gibco BRL, Grand Island, NY) supplemented with 10% fetal bovine serum and 2 mM L-glutamine.

Analysis of HMGB1 release

To determine the effect of VPA on HMGB1 release, RAW-blue cells were stimulated with various concentrations of VPA, *E. coli* LPS, TNF-α, TSA, and SAHA, and the amount of HMGB1 released into the medium was measured by enzyme-linked immunosorbent assay (ELISA) (SHINO-TEST).

Measurement of NF-κB activity

RAW-blue cells were incubated with VPA. Culture supernatants of the cells were mixed with QUANTI-blue (InvivoGen), an alkaline phosphatase substrate, and then incubated for 30 min at 37°C. The absorbance (λ = 595 nm) was measured by using Appliskan (Thermo Fisher Scientific, Waltham, Mass) to detect relative NF-κB activity.

Western blotting

RAW-blue cells were incubated with various specimens for 0.5 to 24 h. Cells were lysed in Celytic M (Sigma-Aldrich) with protease inhibitor mixture (Nacalai Tesque, Kyoto, Japan) and phosphatase inhibitor mixture (Nacalai Tesque). Cell lysates were separated by sodium dodecyl sulfate–polyacrylamide gel electrophoresis and transferred to polyvinylidene difluoride membranes. The membranes were blotted by the SNAP i.d. Protein Detection System (Millipore, Billerica, Mass) following the manufacturer's protocol. The membranes were blocked with 0.02% skim milk (BD Bioscience) in Tris-buffered saline (pH 7.4) containing 0.05% Tween 20 (TBST) and then incubated with the appropriate antibodies in TBST containing 0.02% skim milk. After washing, the membranes were incubated with horseradish peroxidase–conjugated anti-rabbit or mouse IgG antibodies (IBL, Takasaki, Japan) in TBST containing 0.02% skim milk. The membranes were washed twice with TBST, and then immunoreactive bands were visualized using an ECL Plus Detection System (GE Healthcare, Uppsala, Sweden).

Cytotoxicity assay

Cell viability was determined by using Cytotoxity Detection Kit PULS (LDH) (Roche Diagnostics, Basel, Switzerland) following the manufacturer's protocol. As an apoptosis marker, caspase 3/7 activity was determined by the Caspase-Glo 3/7 assay (Promega, Madison, Wis) following the manufacturer's protocol.

Fluorescence immunostaining

To investigate the translocation of HMGB1, RAW-blue cells were cultured on Lab-Tek chamber slides (Nalge Nunc International, Cambridge, Mass) and incubated with each specimen for 24 h. Cells were then fixed with 4% paraformaldehyde for 15 min and permeabilized with 0.2% Triton X-100 in phosphate-buffered saline for 5 min. After washing with phosphate-buffered saline three times, cells were blocked in 5% sheep serum albumin in TBST for 1 h and incubated with rabbit anti-HMGB1 polyclonal antibody (SHINO-TEST) for 1 h at room temperature. The slides were then washed with TBST and incubated with anti–rabbit IgG conjugated with green Alexa Fluor 488 (Invitrogen, Carlsbad, Calif). Finally, the slides were covered by ProLong Gold with DAPI (Invitrogen). Images were captured using a fluorescence microscope (Keyence, Osaka, Japan).

Quantitative polymerase chain reaction

RAW-blue cells were stimulated with 5 mM of VPA for 24 h, and mRNA expression of γ-aminobutyric acid (GABA) receptors was analyzed by reverse transcriptase–polymerase chain reaction (RT-PCR). Total RNA from cells was purified with an RNeasy mini kit (Qiagen, Hombrechtikon, Switzerland) and DNdigest (Qiagen), and cDNA was synthesized using ReverTra Ace (Toyobo, Osaka, Japan) following the manufacturer's protocol. Real-time PCR was performed on a 7300 Real-time PCR System (Applied Biosystems, Carlsbad, Calif) using SYBR MIX Plus (Toyobo). The mouse HMGB1 transcript was amplified using the following primers: forward, 5′-CCA AAG GGG AGA CCA AAA AG-3′; reverse, 5′-TCA TAG GGC TGC TTG TCA TCT-3′. The mouse TNF-α transcript was amplified using the following primers: forward, 5′-AAG CCT GTA GCC CAC GTC GTA-3′; reverse, 5′-GGC ACC ACT AGT TGG TTG TCT TTG-3′. The mouse $GABA_A$ receptor subunit α1 transcript was amplified using the following primers: forward, 5′-CGA AGG TGG CTT ATG CAA CA-3′; reverse, 5′-CCC ACG CAT ACC CTC TCT TG-3′. The mouse $GABA_A$ receptor subunit α3 transcript was amplified using the following primers: forward, 5′-CTC CAA CAG CGA TTG CTT CA-3′; reverse, 5′-TGA TGC GGG AAA TTT TGT CA-3′. The mouse $GABA_A$ receptor subunit β2 transcript was amplified using the following primers: forward, 5′-AAC CGA GTG GCA GAC CAA CT-3′; reverse, 5′-TCG GGA TGC AAT CGA ATC AT-3′. Mouse β-actin transcript was used as an internal control: forward primer, 5′-CAT CCG TAA AGA CCT CTA TGC CAA-3′; reverse, 5′-ATG GAG CCA CCG ATC CAC-3′. The housekeeping gene, β-actin, was used to normalize all test genes, and data quantification was performed using the ΔΔCT method.

Murine model of endotoxemia

This study was approved and performed in accordance with the guidelines of the School of Dentistry, Aichi Gakuin University at Nagoya, Aichi, Japan. Endotoxemia was induced in Balb/c mice (male, 7–8 weeks old) by i.p. injection of *E. coli* LPS (1). Briefly, mice were injected s.c. with VPA (600 mg/kg) 12 h before LPS administration. The mice were monitored for survival over a period of 192 h after LPS administration. In some cases, VPA (600 mg/kg) with or without a neutralizing antibody for HMGB1 (2 or 4 mg/kg) was given to mice 12 h before LPS (25 mg/kg) administration. The mice were monitored for survival over a period of 192 h after LPS administration. In parallel experiments, blood was collected from mice at 24 h after LPS administration, and levels of serum IL-6 (kit purchased from IBL) and HMGB1 (kit purchased from SHINO-TEST) were determined by ELISA.

Statistics

Results are expressed as means ± SD. Mortality studies were analyzed using log-rank test. Statistical evaluation of the continuous data was performed by one-way analysis of variance, followed by Tukey test for between-group comparisons. These statistical analyses were done using the statistical software Statcel 2 (OMS Ltd., Saitama, Japan). The level of significance was considered to be $P < 0.05$.

RESULTS

VPA enhances systemic inflammatory responses induced by LPS in vivo and in vitro

To determine the effect of VPA on systemic inflammatory response *in vivo*, we used a mouse model of endotoxic shock induced by injecting purified *E. coli* LPS according to the modified method of Galanos et al. (20). Valproic acid was injected i.p. 12 h before administering saline or LPS, and the survival rate of the mice was determined. Fifty percent of the mice died within 3 days after administration of LPS (Fig. 1A). Valproic acid alone did not cause lethality in mice (Fig. 1A). However, pretreatment with VPA reduced the survival rate of

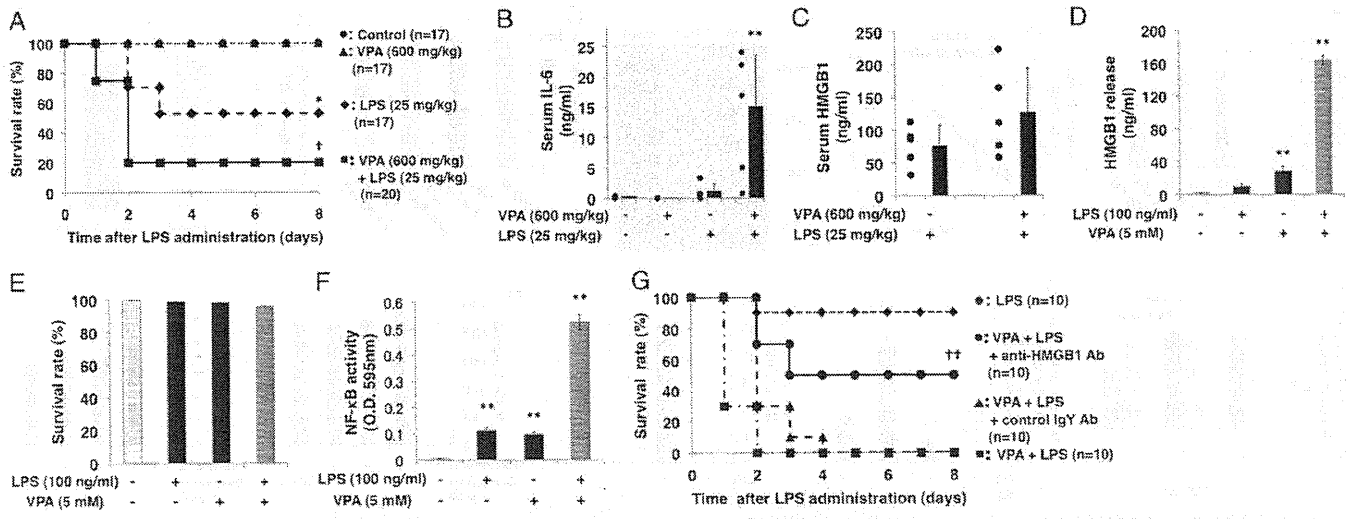

FIG. 1. **Valproic acid enhanced systemic inflammatory responses induced by LPS.** Valproic acid (600 mg/kg; s.c. injection) was given to mice 12 h before LPS administration (25 mg/kg; i.p. injection). Mice were monitored for survival over a period of 192 h after LPS administration (A) ($^{*}P < 0.05$ vs. control, $^{\dagger}P < 0.05$ vs. LPS). Blood in mice was collected at 24 h after LPS administration, and levels of serum IL-6 and HMGB1 were determined by ELISA (B and C) ($^{**}P < 0.01$ vs. control). RAW-blue cells were preincubated with VPA (5 mM) for 6 h and were then treated with LPS (100 ng/mL) for 24 h. The levels of HMGB1 in culture media were determined by ELISA (D) ($^{**}P < 0.01$ vs. control). Cell viability was evaluated by LDH assay (E). Nuclear factor κB activity in RAW-blue cells was analyzed by a reporter assay, as described in Materials and Methods (F) ($^{**}P < 0.01$ vs. control). Valproic acid (600 mg/kg) with or without a neutralizing chicken antibody for HMGB1 (4 mg/kg) and a control IgY antibody was given to mice 12 h before LPS (25 mg/kg) administration. Mice were monitored for survival over a period of 192 h after LPS administration (G) ($^{\dagger\dagger}P < 0.05$ vs. VPA + LPS).

mice (20%) (Fig. 1A). We also determined the concentrations of IL-6 and HMGB1 in serum of the mice. Serum was collected at 24 h after LPS administration, and levels of IL-6 and HMGB1 in the serum were determined by ELISA. Interleukin 6 was induced in serum in LPS-administered mice (Fig. 1B). Pretreatment with VPA significantly increased the concentration of IL-6 in serum in LPS-administered mice (Fig. 1B). Furthermore, serum levels of HMGB1 were increased in VPA-pretreated mice (Fig. 1C).

High-mobility group box 1 is a key mediator of systemic inflammation and sepsis (1). Therefore, we investigated whether VPA affects LPS-induced HMGB1 production in macrophages in culture. RAW-blue cells were preincubated with VPA (5 mM) for 6 h and were then treated with LPS (100 ng/mL) for 24 h. The levels of HMGB1 in culture media were detected by ELISA. Valproic acid as well as LPS induced HMGB1 release in macrophage cultures (Fig. 1D). However, release of HMGB1 significantly increased in cultures pretreated with VPA before stimulation with LPS (Fig. 1D). To exclude the possibility that HMGB1 in media leaks out from necrotic cells, we examined the effect of pretreatment of VPA and LPS stimuli on viability of macrophages. RAW-blue cells were preincubated with VPA (5 mM) for 6 h and were then treated with LPS (100 ng/mL) for 24 h. Cell viability was evaluated by LDH assay. Lipopolysaccharide or VPA alone or in combination did not affect the viability of macrophages (Fig. 1E). We next examined VPA activation of NF-κB in macrophage cultures. Pretreatment with VPA significantly enhanced LPS-induced NF-κB activation (Fig. 1F). To test the effect of HMGB1 blockade in the endotoxin shock mouse model, anti-HMGB1 chicken polyclonal antibodies or control IgY antibodies were injected into the peritoneal cavity simultaneously and after injection of VPA. All 10 mice in the group administered VPA and LPS were dead 2 days after LPS administration. However, when mice subjected to LPS administration were pretreated with anti-HMGB1 antibodies (total 4 mg/kg), 5 (50%) of the 10 mice survived for 8 days (Fig. 1G). In contrast, none of the 10 mice survived after pretreatment with VPA and control antibodies and then administration of LPS (Fig. 1G). These results suggest that VPA primes macrophages to respond to LPS and to produce inflammatory mediators such as HMGB1 and enhances systemic inflammatory responses in mice.

VPA induces HMGB1 release from macrophages

To confirm that VPA activates HMGB1 release, RAW-blue cells were incubated with VPA (5 mM), LPS (100 ng/mL), and TNF-α (20 ng/mL) for 24 h, and the amount of HMGB1 released into the medium was measured by ELISA. Valproic acid strongly induced HMGB1 in macrophage cultures, and the amounts of the protein released were comparable to those induced by *E. coli* LPS (Fig. 2A). Valproic acid–induced HMGB1 release increased time dependently and continued for up to 24 h (Fig. 2B). We next compared the localizations of HMGB1 in VPA-stimulated and nonstimulated macrophages. Strong nuclear localization of HMGB1 was observed in untreated macrophages, whereas nuclear-cytoplasmic translocation of HMGB1 was observed in macrophages stimulated with VPA, LPS, and TNF-α for 24 h (Fig. 2C). To determine whether VPA induces active HMGB1 release in the absence of cell death, the effects of VPA on cell viability were investigated by LDH assay. Valproic acid as well as LPS and TNF-α was not toxic to macrophages in culture (Fig. 2D). To determine the effect of VPA on the apoptosis pathway, we examined the activity of caspase 3/7 in VPA-treated macrophage cultures. Activity of caspase 3/7 was not increased by stimulation with VPA in macrophages (Fig. 2E). Moreover, VPA did not induce mRNA expression of HMGB1 in macrophages (Fig. 2F). We also examined mRNA expressions of HMGB1

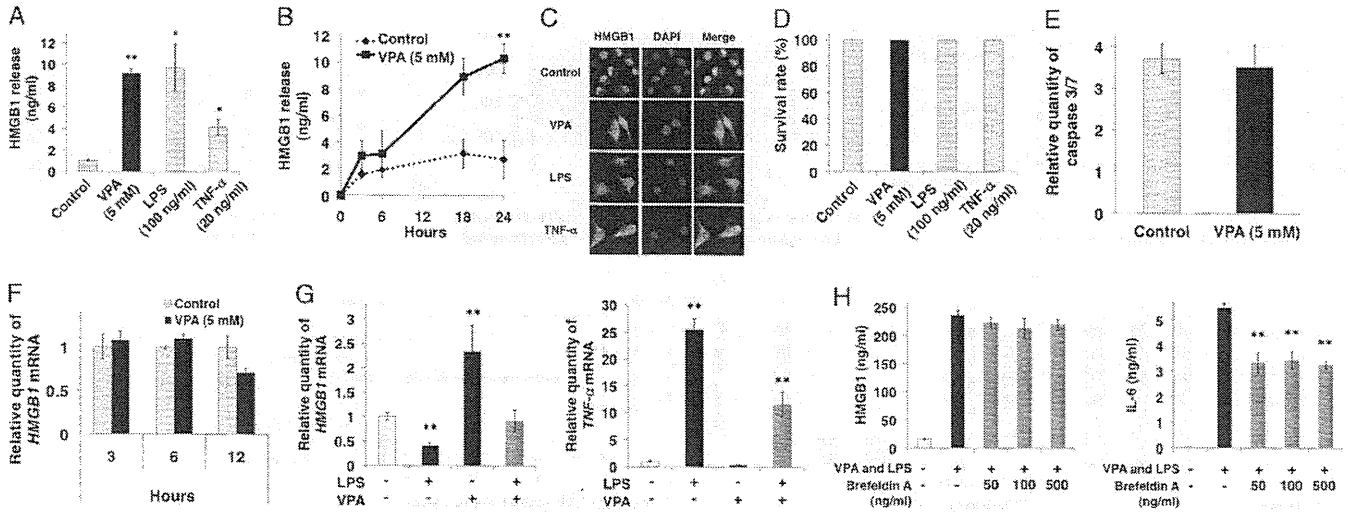

FIG. 2. **VPA induced HMGB1 release from macrophages.** RAW-blue cells were incubated with VPA (5 mM), LPS (100 ng/mL), and TNF-α (20 ng/mL) for 24 h (A). RAW-blue cells were incubated with VPA (5 mM) for 3, 6, 18, and 24 h (B). HMGB1 levels in supernatants were analyzed by ELISA (A and B). Translocation of HMGB1 in response to VPA (5 mM), LPS (100 ng/mL), and TNF-α (20 ng/mL) 24 h was analyzed by immunofluorescence assay (C). Cell viability was evaluated by LDH assay (D). Caspase 3/7 activity in the cells was analyzed by using a detection kit (E). Levels of *HMGB1* mRNA expresion were analyzed by real-time PCR and are shown as relative expression normalized by the levels of a housekeeping gene (*β-actin*) mRNA (F) (n = 3 ± SD, $*P < 0.05$ vs. control, $**P < 0.01$ vs. control). RAW-Blue cells were pre-incubated with Brefeldin A (50–500 ng/ml) for 3 h and were then treated with VPA (5 mM) and LPS (100 ng/ml) for 24 h. The levels of HMGB1 and IL-6 in culture media were determined by ELISA (H). (n = 3 ± S.D. $**P < 0.01$ vs. VPA and LPS).

and TNF-α by stimulations with LPS and VPA. Stimulation with VPA for 24 h increased steady-state levels of HMGB1 mRNA. However, LPS did not induce HMGB1 mRNA expression at a concentration of 100 ng/mL (Fig. 2G). High-mobility group box 1 mRNA levels also did not increase in RAW-blue cells primed with VPA and then stimulated with TNF-α. On the other hand, LPS strongly induced mRNA expression of TNF-α in RAW-blue cells (Fig. 2G). However, VPA did not induce its expression. These results suggest that HMGB1 release by stimulation with VPA due not to cell lysis or injury but to an active process that is not dependent on increase in gene expression and mRNA induction of HMGB1 by VPA is not due to activation of NF-κB. We also examined the effect of brefeldin A, a blocker of membrane export of proteins out of the endoplasmic reticulum, on release of HMGB1 induced by VPA and LPS. As shown in Figure 2H, the release of HMGB1 stimulated with VPA and LPS did not suppress by addition of brefeldin A, although the release of IL-6 stimulated with these stimulants suppressed with it at a concentration of 50 ng/ml. These results suggest that HMGB1 release with VPA and LPS were not due to the conventional secretory pathway.

ERK kinase may play a role in VPA-induced HMGB1 release

To clarify the mechanism by which VPA induces the release of HMGB1, we examined whether MAP kinases mediate VPA-induced HMGB1 release. Treatment of macrophages with VPA for 0.5 or 24 h activated phosphorylation of ERK (Fig. 3A). However, VPA did not induce phosphorylation of JNK and p38. In contrast, LPS induced phosphorylation of ERK, JNK, and p38. Inhibition of ERK with PD98059 suppressed VPA-induced ERK phosphorylation and HMGB1 release by macrophages (Fig. 3B and Supplemental Digital Content 5, at http://links.lww.com/SHK/A90). Valproic acid also induced NF-κB activation in macrophages (Fig. 3C), and it was inhibited by treatment with PD98059 (Fig. 3D). These findings suggest that VPA stimulates the release of HMGB1 from activated macrophages via ERK MAP kinase and NF-κB signaling. A recent study showed that acetylation of cytosolic HMGB1 triggers its exocytosis from monocytic cells (21).

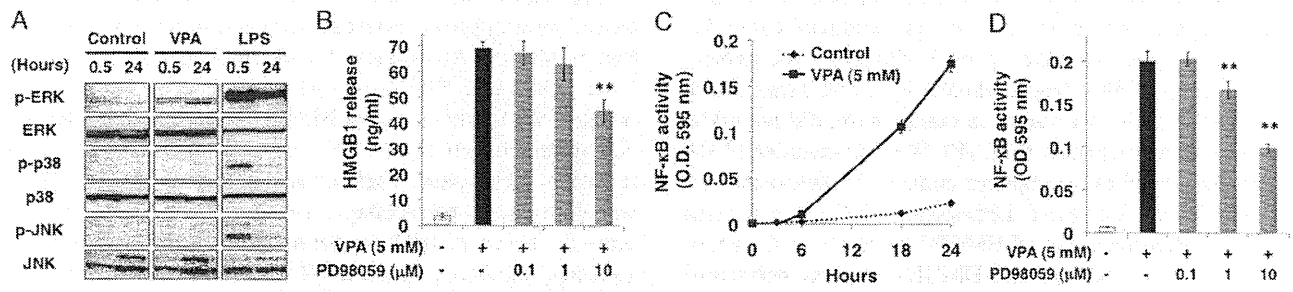

FIG. 3. **ERK kinase mediates VPA-induced HMGB1 release.** RAW-blue cells were incubated with VPA (5 mM) and LPS (100 ng/mL) for 0.5 to 24 h. Phosphorylation of p38MAPK, ERK1/2, and JNK was assayed by Western blot analysis (A). RAW-blue cells were incubated with VPA (5 mM) and PD98059 (0.1–10 μM) for 24 h. The levels of HMGB1 in culture supernatants were analyzed by ELISA (B). RAW-blue cells were incubated with VPA (5 mM) for 3, 6, 18, and 24 h (C). RAW-blue cells were incubated with VPA (5 mM) and PD98059 (0.1–10 μM) for 24 h (D). The levels of NF-κB activation were analyzed by reporter assay, as described in Materials and Methods (C and D) (n = 3 ± SD, $**P < 0.01$ vs. VPA).

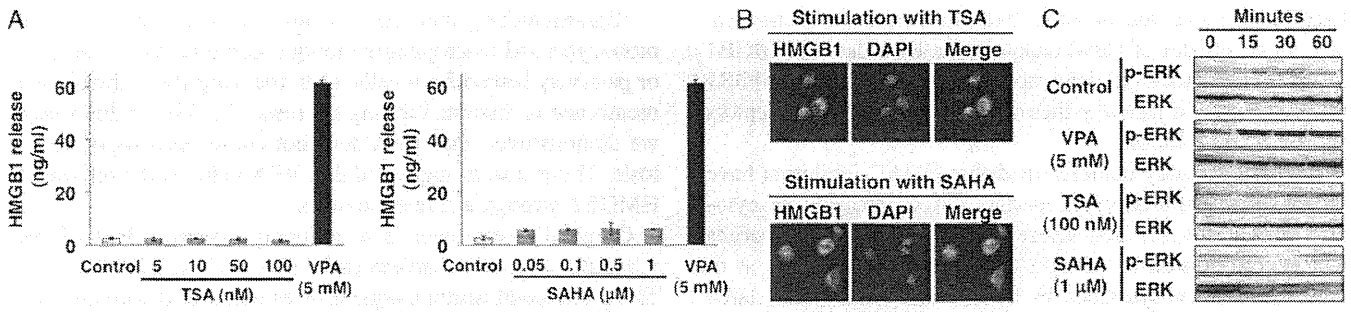

FIG. 4. **Histone deacetylases do not mediate the effects of VPA on HMGB1 release.** RAW-blue cells were incubated in histone deacetylase inhibitors TSA (5–100 nM) or SAHA (0.05–1 μM) for 24 h. The levels of HMGB1 in supernatants were evaluated by ELISA (A). Translocation of HMGB1 in response to TSA (100 nM) and SAHA (1 μM) for 24 h was analyzed by immunofluorescence assay (B). RAW-blue cells were incubated with VPA (5 mM), TSA (100 nM), and SAHA (1 μM) for 0 to 1 h. Phosphorylation of ERK1/2 was assayed by Western blot analysis (C) (n = 3 ± SD).

HDACs do not mediate the effects of VPA on HMGB1 release

Therefore, we examined the effects of TSA and SAHA, inhibitors of HDAC, on VPA-induced HMGB1 release in macrophage cultures. Trichostatin A and SAHA did not induce HMGB1 release from macrophages (Fig. 4A). In addition, HMGB1 was retained in nuclear regions, and the levels of HMGB1 in the cytoplasmic region were not increased after treatment with TSA and SAHA (Fig. 4B). Furthermore, TSA and SAHA did not activate phosphorylation of ERK, although VPA activated phosphorylation of ERK in the same conditions (Fig. 4C). These results suggest that VPA-induced HMGB1 release is not due to its inhibitory effect on HDACs.

VPA activates GABA signaling

Valproic acid exerts its antiepileptic effect principally by elevating GABA concentration in the brain (22, 23). Therefore, we next examined whether VPA increases GABA concentration in macrophage cultures. RAW-blue cells were stimulated with 5 mM of VPA for 24 h. γ-Aminobutyric acid levels in the cytoplasm and supernatants were analyzed by ELISA. Valproic acid induced GABA release into media (Figures 1A and B, Supplemental Digital Content 1, at http://links.lww.com/SHK/A85, and Supplemental Digital Content 2, at http://links.lww.com/SHK/A86). RAW cells were stimulated with VPA (5 mM) for 24 h. γ-Aminobutyric acid levels in supernatants (A) and cytoplasms (B) were analyzed by ELISA (n = 3 ± SD). We then confirmed that GABA release from macrophages acts on macrophages through a paracrine pathway and induces HMGB1 release. We examined the effect of GABA on HMGB1 release in macrophages. γ-Aminobutyric acid at concentrations of 1 to 1,000 μM did not activate the release of HMGB1 (Figures 2A and B, Supplemental Digital Content 3, at http://links.lww.com/SHK/A87, and Supplemental Digital Content 4, at http://links.lww.com/SHK/A88). RAW cells were stimulated with various concentrations (1–1,000 μM) of GABA for 24 h. High-mobility group box 1 levels in supernatants were analyzed by ELISA (A). Cell viability was evaluated by LDH assay (B) (n = 3 ± SD). These findings suggest that GABA did not mediate HMGB1 release induced by VPA.

Next, we examined whether VPA induces expression of GABA receptors in macrophages. RAW cells were stimulated with 5 mM of VPA for 24 h, and expression of $GABA_A$ receptor subunits in murine macrophages was investigated by quantitative RT-PCR. Among the α and β subunits, the β_2 subunit was expressed in macrophages (Fig. 5A). Expression of the α_1 and α_3 subunits of the $GABA_A$ receptor was induced by stimulation with 5 mM of VPA (Fig. 5A). Expression of α_2, α_4, α_5, and β_1 was not detected in macrophages with or without VPA stimulation (Fig. 5A). Picrotoxin, a $GABA_A$ receptor antagonist, inhibited VPA-induced HMGB1 release at a concentration of 0.5 μM (Fig. 5B). Picrotoxin also inhibited the activation of ERK phosphorylation by stimulation with VPA in macrophages (Fig. 5C). These results suggest that VPA induces HMGB1 release in macrophages in part through activation of $GABA_A$ receptors and ERK kinase.

DISCUSSION

In the present study, we demonstrated that VPA significantly augmented the proinflammatory response induced by

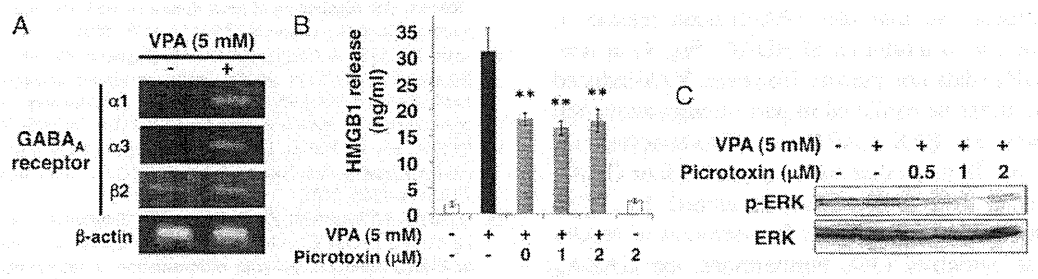

FIG. 5. **Valproic acid induced HMGB1 release by activating the $GABA_A$ receptor.** RAW-blue cells were stimulated with VPA (5 mM) for 24 h. Expression of $GABA_A$ receptor mRNA was analyzed by RT-PCR (A).RAW-blue cells were incubated with VPA (5 mM) in the presence or absence of picrotoxin (2 μM) for 24 h. The levels of HMGB1 in supernatants were analyzed by ELISA (B). Phosphorylation of ERK1/2 was detected by Western blot analysis (C) (n = 3 ± SD, $^{**}P < 0.01$ vs. VPA).

LPS both *in vivo* and *in vitro*. Valproic acid reduced survival in a mouse model of lethal endotoxemia by inducing HMGB1 release. Pharmacologic data show that VPA induces HMGB1 release through a pathway that might include GABA receptors and ERK MAP kinase.

A previous study demonstrated that HDAC inhibitors have broad anti-inflammatory properties via suppression of cytokine production (6, 24). These anti-inflammatory properties were demonstrated *in vitro* by inhibition of the secretion of proinflammatory cytokines in LPS- and cytokine-stimulated peripheral blood mononuclear cells (PBMCs) and in macrophages (6). Histone deacetylase inhibitors reduced circulating cytokine concentrations during endotoxemia in mice (25). Histone deacetylase inhibitors, by increasing the levels of histone acetylation, can lead to a local alteration in the structure of chromatin, which facilitates gene-specific repression of transcription. Therefore, HDAC inhibition is a relevant mechanism mediating anti-inflammatory effects.

How do HDACs and HDAC inhibitors regulate inflammation? Histone deacetylases were originally identified as enzymes that modify acetylation of histone proteins, thereby regulating gene expression. However, subsequent research has identified many other targets of acetylation, and acetylation of nonhistone proteins regulates a variety of other cell signaling pathways, including inflammation. Thus, at least three distinct pathways may exist for HDAC regulation of inflammation. First, HDACs might regulate gene expression of inflammatory mediators through modification of histone proteins. Second, HDACs might regulate transcription factors such as NF-κB that transactivate proinflammatory genes. Third, HDACs directly modify members of the mitogen-activated protein kinase (MAPK) pathway, such as MAPK phosphatase-1 (MKP-1), which in turn modulate transcription factors controlling innate immune responses (12).

Valproic acid is an HDAC inhibitor of the class of short-chain fatty acids, and it exhibited anti-inflammatory effects through histone hyperacetylation (16, 26). On the other hand, several mechanisms are known to promote the relocation of HMGB1 from the nucleus to cytoplasm, including the acetylation (21, 27) and phosphorylation (28) of HMGB1 and the destabilized association of HMGB1 with chromatin or a nuclear import protein (28). High-mobility group box 1 has been reported to be a substrate of histone acetylase, and it has been shown that HDAC inhibitors induce the relocation of HMGB1 from the nucleus to cytoplasm (21, 27). In this study, we demonstrated that VPA induced HMGB1 release in macrophage cultures and that the VPA-induced release of HMGB1 was not due to inhibition of HDAC (Fig. 4) or acetylation of HMGB1 (data not shown). However, VPA-induced HMGB1 release might be mediated in part through activation of GABA receptors and ERK MAP kinase. This conclusion is strengthened by our findings that inhibitors of ERK or GABA receptors abolished HMGB1 release stimulated by VPA. Phosphorylation of ERK is important for secretion of insulin (29) and various cytokines (30). Furthermore, the $GABA_A$ receptor regulates the phosphorylation of ERK. Therefore, our studies support the theory that MAPK signaling and GABA signaling mediate VPA activation of HMGB1 release.

High-mobility group box 1 is either secreted from activated monocytes and macrophages through secretory lysosomes (31) or passively leaked from cells when the integrity of the plasma membrane is disrupted during necrosis (32, 33). In this study, we demonstrated that VPA does not cause necrosis or apoptosis. These results suggested that VPA induced the release of HMGB1 through active exocytosis.

Gingival overgrowth is a common adverse effect of the administration of an antiepileptic drug such as VPA (19, 34). The presence of dental plaque is often associated with gingival overgrowth (35). Morphological changes in the gingiva lead to the retention of dental plaque. Bacterial components, such as LPS and lipoprotein, in dental plaque can be recognized by host cell Toll-like receptors and play an important role in the inflammatory response in periodontal tissue. Higher levels of HMGB1 were shown to be present in gingival crevicular fluid from periodontal patients (36). High-mobility group box 1 potentiates the action of LPS (37), and thus release of HMGB1 induced by VPA may exaggerate the outcome of bacterial insult in periodontal tissue.

REFERENCES

1. Wang H, Bloom O, Zhang M, Vishnubhakat JM, Ombrellino M, Che J, Frazier A, Yang H, Ivanova S, Borovikova L, et al.: HMG-1 as a late mediator of endotoxin lethality in mice. *Science* 285:248–251, 1999.
2. Gotfryd K, Skladchikova G, Lepekhin EA, Berezin V, Bock E, Walmod PS: Cell type–specific anti-cancer properties of valproic acid: independent effects on HDAC activity and Erk1/2 phosphorylation. *BMC Cancer* 10:383, 2010.
3. Zhu K, Qu D, Sakamoto T, Fukasawa I, Hayashi M, Inaba N: Telomerase expression and cell proliferation in ovarian cancer cells induced by histone deacetylase inhibitors. *Arch Gynecol Obstet* 277:15–19, 2008.
4. Duenas-Gonzalez A, Candelaria M, Perez-Plascencia C, Perez-Cardenas E, de la Cruz-Hernandez E, Herrera LA: Valproic acid as epigenetic cancer drug: preclinical, clinical and transcriptional effects on solid tumors. *Cancer Treat Rev* 34:206–222, 2008.
5. Hrzenjak A, Moinfar F, Kremser ML, Strohmeier B, Petru E, Zatloukal K, Denk H: Histone deacetylase inhibitor vorinostat suppresses the growth of uterine sarcomas *in vitro* and *in vivo*. *Mol Cancer* 9:49, 2010.
6. Halili MA, Andrews MR, Labzin LI, Schroder K, Matthias G, Cao C, Lovelace E, Reid RC, Le GT, Hume DA, et al.: Differential effects of selective HDAC inhibitors on macrophage inflammatory responses to the Toll-like receptor 4 agonist LPS. *J Leukoc Biol* 87:1103–1114, 2010.
7. Faraco G, Pittelli M, Cavone L, Fossati S, Porcu M, Mascagni P, Fossati G, Moroni F, Chiarugi A: Histone deacetylase (HDAC) inhibitors reduce the glial inflammatory response *in vitro* and *in vivo*. *Neurobiol Dis* 36:269–279, 2009.
8. Han SB, Lee JK: Anti-inflammatory effect of trichostatin-A on murine bone marrow-derived macrophages. *Arch Pharm Res* 32:613–624, 2009.
9. Kim HJ, Rowe M, Ren M, Hong JS, Chen PS, Chuang DM: Histone deacetylase inhibitors exhibit anti-inflammatory and neuroprotective effects in a rat permanent ischemic model of stroke: multiple mechanisms of action. *J Pharmacol Exp Ther* 321:892–901, 2007.
10. Reilly CM, Mishra N, Miller JM, Joshi D, Ruiz P, Richon VM, Marks PA, Gilkeson GS: Modulation of renal disease in MRL/lpr mice by suberoylanilide hydroxamic acid. *J Immunol* 173:4171–4178, 2004.
11. Leoni F, Zaliani A, Bertolini G, Porro G, Pagani P, Pozzi P, Dona G, Fossati G, Sozzani S, Azam T, et al.: The antitumor histone deacetylase inhibitor suberoylanilide hydroxamic acid exhibits antiinflammatory properties via suppression of cytokines. *Proc Natl Acad Sci U S A* 99:2995–3000, 2002.
12. Cao W, Bao C, Padalko E, Lowenstein CJ: Acetylation of mitogen-activated protein kinase phosphatase-1 inhibits Toll-like receptor signaling. *J Exp Med* 205:1491–1503, 2008.
13. Gottlicher M, Minucci S, Zhu P, Kramer OH, Schimpf A, Giavara S, Sleeman JP, Lo Coco F, Nervi C, Pelicci PG, et al.: Valproic acid defines a novel class of HDAC inhibitors inducing differentiation of transformed cells. *EMBO J* 20:6969–6978, 2001.
14. Herranz JL, Armijo JA, Arteaga R: Clinical side effects of phenobarbital, primidone, phenytoin, carbamazepine, and valproate during monotherapy in children. *Epilepsia* 29:794–804, 1988.

15. Blaheta RA, Cinatl J Jr: Anti-tumor mechanisms of valproate: a novel role for an old drug. *Med Res Rev* 22:492–511, 2002.
16. Ichiyama T, Okada K, Lipton JM, Matsubara T, Hayashi T, Furukawa S: Sodium valproate inhibits production of TNF-alpha and IL-6 and activation of NF-kappaB. *Brain Res* 857:246–251, 2000.
17. Garnier R, Boudignat O, Fournier PE: Valproate poisoning. *Lancet* 2:97, 1982.
18. El-Mowafy AM, Abdel-Dayem MA, Abdel-Aziz A, El-Azab MF, Said SA: Eicosapentaenoic acid ablates valproate-induced liver oxidative stress and cellular derangement without altering its clearance rate: dynamic synergy and therapeutic utility. *Biochim Biophys Acta* 1811:460–467, 2011.
19. Anderson HH, Rapley JW, Williams DR: Gingival overgrowth with valproic acid: a case report. *ASDC J Dent Child* 64:294–297, 1997.
20. Galanos C, Roppel J, Weckesser J, Rietschel ET, Mayer H: Biological activities of lipopolysaccharides and lipid A from Rhodospirillaceae. *Infect Immun* 16:407–412, 1977.
21. Bonaldi T, Talamo F, Scaffidi P, Ferrera D, Porto A, Bachi A, Rubartelli A, Agresti A, Bianchi ME: Monocytic cells hyperacetylate chromatin protein HMGB1 to redirect it towards secretion. *EMBO J* 22:5551–5560, 2003.
22. Nau H, Loscher W: Valproic acid: brain and plasma levels of the drug and its metabolites, anticonvulsant effects and gamma-aminobutyric acid (GABA) metabolism in the mouse. *J Pharmacol Exp Ther* 220:654–659, 1982.
23. Guidotti A, Auta J, Chen Y, Davis JM, Dong E, Gavin DP, Grayson DR, Matrisciano F, Pinna G, Satta R, et al.: Epigenetic GABAergic targets in schizophrenia and bipolar disorder. *Neuropharmacology* 60:1007–1016, 2011.
24. Halili MA, Andrews MR, Sweet MJ, Fairlie DP: Histone deacetylase inhibitors in inflammatory disease. *Curr Top Med Chem* 9:309–319, 2009.
25. Roger T, Lugrin J, Le Roy D, Goy G, Mombelli M, Koessler T, Ding XC, Chanson AL, Knaup Reymond M, Miconnet I, et al.: Histone deacetylase inhibitors impair innate immune responses to Toll-like receptor agonists and to infection. *Blood* 117:1205–1217, 2011.
26. Zhang Z, Zhang ZY, Fauser U, Schluesener HJ: Valproic acid attenuates inflammation in experimental autoimmune neuritis. *Cell Mol Life Sci* 65:4055–4065, 2008.
27. Carneiro VC, de Moraes Maciel R, de Abreu da Silva IC, da Costa RF, Paiva CN, Bozza MT, Fantappie MR: The extracellular release of *Schistosoma mansoni* HMGB1 nuclear protein is mediated by acetylation. *Biochem Biophys Res Commun* 390:1245–1249, 2009.
28. Youn JH, Shin JS: Nucleocytoplasmic shuttling of HMGB1 is regulated by phosphorylation that redirects it toward secretion. *J Immunol* 177:7889–7897, 2006.
29. Persaud SJ, Wheeler-Jones CP, Jones PM: The mitogen-activated protein kinase pathway in rat islets of Langerhans: studies on the regulation of insulin secretion. *Biochem J* 313:119–124, 1996.
30. Kawahara K, Biswas KK, Unoshima M, Ito T, Kikuchi K, Morimoto Y, Iwata M, Tancharoen S, Oyama Y, Takenouchi K, et al.: C-reactive protein induces high-mobility group box-1 protein release through activation of p38MAPK in macrophage RAW264.7 cells. *Cardiovasc Pathol* 17:129–138, 2008.
31. Gardella S, Andrei C, Ferrera D, Lotti LV, Torrisi MR, Bianchi ME, Rubartelli A: The nuclear protein HMGB1 is secreted by monocytes via a non-classical, vesicle-mediated secretory pathway. *EMBO Rep* 3:995–1001, 2002.
32. Scaffidi P, Misteli T, Bianchi ME: Release of chromatin protein HMGB1 by necrotic cells triggers inflammation. *Nature* 418:191–195, 2002.
33. Bianchi ME, Manfredi AA: High-mobility group box 1 (HMGB1) protein at the crossroads between innate and adaptive immunity. *Immunol Rev* 220:35–46, 2007.
34. Seymour RA, Smith DG, Turnbull DN: The effects of phenytoin and sodium valproate on the periodontal health of adult epileptic patients. *J Clin Periodontol* 12:413–419, 1985.
35. Seymour RA, Ellis JS, Thomason JM: Risk factors for drug-induced gingival overgrowth. *J Clin Periodontol* 27:217–223, 2000.
36. Morimoto Y, Kawahara KI, Tancharoen S, Kikuchi K, Matsuyama T, Hashiguchi T, Izumi Y, Maruyama I: Tumor necrosis factor-alpha stimulates gingival epithelial cells to release high mobility-group box 1. *J Periodontal Res* 43:76–83, 2008.
37. Qin YH, Dai SM, Tang GS, Zhang J, Ren D, Wang ZW, Shen Q: HMGB1 enhances the proinflammatory activity of lipopolysaccharide by promoting the phosphorylation of MAPK p38 through receptor for advanced glycation end products. *J Immunol* 183:6244–6250, 2009.

TISSUE ENGINEERING: Part A
Volume 17, Numbers 15 and 16, 2011

DOI: 10.1089/ten.tea.2010.0615

Complete Pulp Regeneration After Pulpectomy by Transplantation of CD105$^+$ Stem Cells with Stromal Cell-Derived Factor-1

Koichiro Iohara, Ph.D.,[1] Kiyomi Imabayashi, Ph.D.,[1] Ryo Ishizaka, D.D.S.,[1,2] Atsushi Watanabe, Ph.D.,[3] Junichi Nabekura, Ph.D.,[4] Masataka Ito, Ph.D.,[5] Kenji Matsushita, Ph.D.,[1] Hiroshi Nakamura, Ph.D.,[6] and Misako Nakashima, Ph.D.[1]

Loss of pulp due to caries and pulpitis leads to loss of teeth and reduced quality of life. Thus, there is an unmet need for regeneration of pulp. A promising approach is stem cell therapy. Autologous pulp stem/progenitor (CD105$^+$) cells were transplanted into a root canal with stromal cell-derived factor-1 (SDF-1) after pulpectomy in mature teeth with complete apical closure in dogs. The root canal was successfully filled with regenerated pulp including nerves and vasculature by day 14, followed by new dentin formation along the dentinal wall. The newly regenerated tissue was significantly larger in the transplantation of pulp CD105$^+$ cells with SDF-1 compared with those of adipose CD105$^+$ cells with SDF-1 or unfractionated total pulp cells with SDF-1. The pulp CD105$^+$ cells highly expressed angiogenic/neurotrophic factors compared with other cells and localized in the vicinity of newly formed capillaries after transplantation, demonstrating its potent trophic effects on neovascularization. Two-dimensional electrophoretic analyses and real-time reverse transcription–polymerase chain reaction analyses demonstrated that the qualitative and quantitative protein and mRNA expression patterns of the regenerated pulp were similar to those of normal pulp. Thus, this novel stem cell therapy is the first demonstration of complete pulp regeneration, implying novel treatment to preserve and save teeth.

Introduction

DENTAL PULP has many functions, and it is essential for longevity of teeth and quality of life. The long-term goal of endodontic treatment after deep caries and/or pulp inflammation is the conservation and restoration of teeth including dental pulp. A promising approach for it is stem-cell-based therapy to regenerate the dentin-pulp complex for the conservation and total restoration of structure and function.[1] The regeneration and tissue engineering of pulp is based on morphogens and growth factors, responding stem/progenitor cells, and the extracellular matrix scaffold.[2] The regeneration of dental pulp in immature teeth with incomplete apical closure has been reported using fibrin in the blood clot or collagen.[3,4] However, there have been no reports concerning total pulp regeneration in mature teeth with complete apical closure by stem/progenitor cell therapy. There is an intimate association of innervation with vasculature of the dental pulp. Angiogenesis/vasculogenesis and neurogenesis are critical for total functional pulp regeneration. The type III receptor of the transforming growth factor-β receptor family cell surface antigen CD105 (endoglin) was selected on the basis of its wide expression on mesenchymal stem cells (MSCs).[5] The stromal cell-derived factor-1 (SDF-1)/CXCR4 axis is present and functional in MSC populations.[6,7] CD105$^+$ stem/progenitor cells from human pulp tissue containing CXCR4-positive cells demonstrated angiogenic/vasculogenic and neurogenic potential.[8] Endothelial cells release SDF-1 under hypoxic conditions and promote cell survival and neovascularization by recruitment and perivascular retention of CXCR4-positive bone marrow-derived cells.[9,10] Therefore, in this study, autologous pulp CD105$^+$ cells were transplanted with SDF-1 in a collagen scaffold into the root canal of mature teeth induced complete apical closure after pulpectomy, in dogs. Thus, we demonstrate for the first time complete pulp regeneration in the root canal, by protein profiles and mRNA expression patterns.

[1]Department of Dental Regenerative Medicine, Center of Advanced Medicine for Dental and Oral Diseases, National Center for Geriatrics and Gerontology, Research Institute, Obu, Aichi, Japan.
[2]Department of Pediatric Dentistry, School of Dentistry, Aichi-gakuin University, Nagoya, Aichi, Japan.
[3]Department of Cognitive Brain Science, National Center for Geriatrics and Gerontology, Research Institute, Obu, Aichi, Japan.
[4]Department of Developmental Physiology, National Institute for Physiological Sciences, Okazaki, Aichi, Japan.
[5]Department of Developmental Anatomy and Regenerative Medicine, National Defense Medical College, Tokorozawa, Saitama, Japan.
[6]Department of Endodontology, School of Dentistry, Aichigakuin University, Nagoya, Aichi, Japan.

Materials and Methods

Cell isolation

Dental pulp cells were separated from pulp tissues of maxillary teeth in dogs as previously described.[11] Primary adipose cells were also separated from the adipose tissue of the same dog as a control. Those primary cells, $2–5 \times 10^5$ cells each were stained with anti-mouse IgG1 negative control (W3/25) (AbD Serotec), mouse IgG1 negative control (Phycoerythrin [PE]) (MCA928PE) (AbD Serotec), and mouse anti-human CD105 (PE) (43A3) (BioLegend), 10 μL per 10^6 cells for 90 min at 4°C, and were sorted by a flow cytometer JSAN (Bay Bioscience). Both $CD105^+$ cells and $CD105^-$ cells derived from the pulp and adipose tissue and total pulp cells without cell fractionation were cultured in EBM2 (Cambrex Bio Science) supplemented with 10 ng/mL IGF (Cambrex Bio Science), 5 ng/mL EGF (Cambrex Bio Science), and 10% FBS (Invitrogen Corporation) to maintain the cells. They were subcultured after reaching 60%–70% confluence.

The phenotype of pulp $CD105^+$ cells was further characterized by flowcytometry at the third passage of culture in comparison with adipose $CD105^+$ cells and unfractionated total pulp cells after immunolabeling with antigen surface markers (Supplementary Material; Supplementary Data are available online at www.liebertonline.com/tea). The experiments were repeated nine times.

Real-time reverse transcription-polymerase chain reaction analysis

To further characterize the phenotype of the cell populations, total RNA were extracted using Trizol (Invitrogen) from the pulp and adipose $CD105^+$ cells and total pulp cells at the third passage. The number of these cells was normalized to 5×10^4 cells in each experiment. First-strand cDNA syntheses were performed from total RNA by reverse transcription using the ReverTra Ace-α (Toyobo). Real-time reverse transcription–polymerase chain reaction (RT-PCR) amplifications were performed at 95°C for 10 s, 62°C for 15 s, and 72°C for 8 s using stem cell markers, canine *CXCR4, Sox2, Stat3, Bmi1, and Rex1* (Supplementary Table S1) labeled with Light Cycler-Fast Start DNA master SYBR Green I (Roche Diagnostics) in Light Cycler (Roche Diagnostics). The design of the oligonucleotide primers was based on published canine cDNA sequences. When canine sequences were not available, human sequences were used. To examine mRNA expression of angiogenic and neurotrophic factors, real-time RT-PCR amplifications of canine *matrix metalloproteinase-3 (MMP-3), VEGF-A, granulocyte-monocyte colony-stimulating factor (GM-CSF), SDF-1, nerve growth factor (NGF), brain-derived neurotrophic factor (BDNF), Neuropeptide Y, Neurotrophin 3, E-selectin, VCAM 1, rhombotin 2, ECSCR,* and *SLC6A6* were also performed (Supplementary Table S1). The RT-PCR products were confirmed by sequencing based on published cDNA sequences. The expression in pulp $CD105^+$ cells and adipose $CD105^+$ cells was compared with that in total pulp cells at the third passage of culture after normalizing with β-*actin*.

Induced differentiation

The differentiation of pulp $CD105^+$ cells from the third to fifth passage, into adipogenic, angiogenic, neurogenic, and odontogenic/osteogenic lineages, was determined and compared with adipose $CD105^+$ cells and unfractionated pulp cells as previously described.[12]

Proliferation and migration assay

To determine cell proliferation in response to SDF1 (Acris), pulp $CD105^+$ cells were compared with total pulp cells and adipose $CD105^+$ cells at fourth passage at the 10^3 cells per 96 well in EBM2 supplemented with 0.2% bovine serum albumin (Sigma) and SDF-1 (50 ng/mL). Ten microliters of Tetracolor one® (Seikagaku Kogyo) was added to the 96-well plate, and cell numbers were measured at 2, 12, 24, and 36 h of culture using a spectrophotometer at 450 nm absorbance. Wells without cells served as negative controls.

To examine migration activity of pulp $CD105^+$ cells by SDF-1, horizontal chemotaxis assay was performed and compared with total pulp cells and adipose $CD105^+$ cells. The TAXIScan-FL (Effector Cell Institute) was used to detect real-time horizontal chemotaxis of cells. The TAXIScan-FL consists of an etched silicon substrate and a flat glass plate, both of which form two compartments with a 6 μm deep microchannel. Each cell fraction (1 μL of 10^5cells/mL) was placed into the single hole with which the device is held together with a stainless steel holder, and 1 μL of 10 ng/μL of SDF-1 was placed into the contra-hole. The video images of cell migration were taken for 6 h.

In vivo *transplantation studies*

An experimental model of whole pulp removal and transplantation of cell populations for regeneration was established in the permanent teeth in dogs to achieve complete apical closure (Narc). The whole pulp removal was carried out in both sides of upper second incisors and lower third incisors under intravenously administered sodium pentobarbital (Schering-Plough) followed by enlargement of apical foramen, 0.7 mm in width using #70 K-file (MANI). Autologous transplantation of the pulp $CD105^+$ cells, adipose $CD105^+$ cells, or total pulp cells, 1×10^6cells in each, from the third to fourth passage, after DiI labeling was performed with collagen TE, a mixture of collagen type I and type III (Nitta Gelatin) in the lower part of the root canals. The upper part of the root canals was further filled with SDF-1 at the final concentration of 15 ng/μL, with collagen TE. The cavity was sealed with zinc phosphate cement (Elite Cement, GC) and composite resin (Clearfil FII) after treatment with a bonding agent (Clearfil Mega Bond). Sixty teeth from 15 dogs were used. Ten teeth transplanted with pulp $CD105^+$ cells with SDF-1, 5 teeth transplanted with adipose $CD105^+$ cells with SDF-1, 5 teeth transplanted with total pulp cells with SDF-1, 5 teeth with SDF-1 only without cells, 5 teeth with pulp $CD105^+$ cells only without SDF-1, and 5 teeth with a scaffold only without cells were harvested for histology after 14 days. Six teeth transplanted with pulp $CD105^+$ cells with SDF-1 were harvested for two-dimensional electrophoretic analyses after 28 days. Four teeth each transplanted with pulp $CD105^+$ cells with SDF-1, adipose $CD105^+$ cells with SDF-1, and total pulp cells with SDF-1 were harvested after 90 days, respectively. Seven normal teeth without any operation were used as control. For morphological analyses, they were fixed in 4% paraformaldehyde (Nakarai Tesque) at 4°C overnight and embedded in paraffin wax (Sigma) after demineralization with 10% formic acid. The paraffin sections

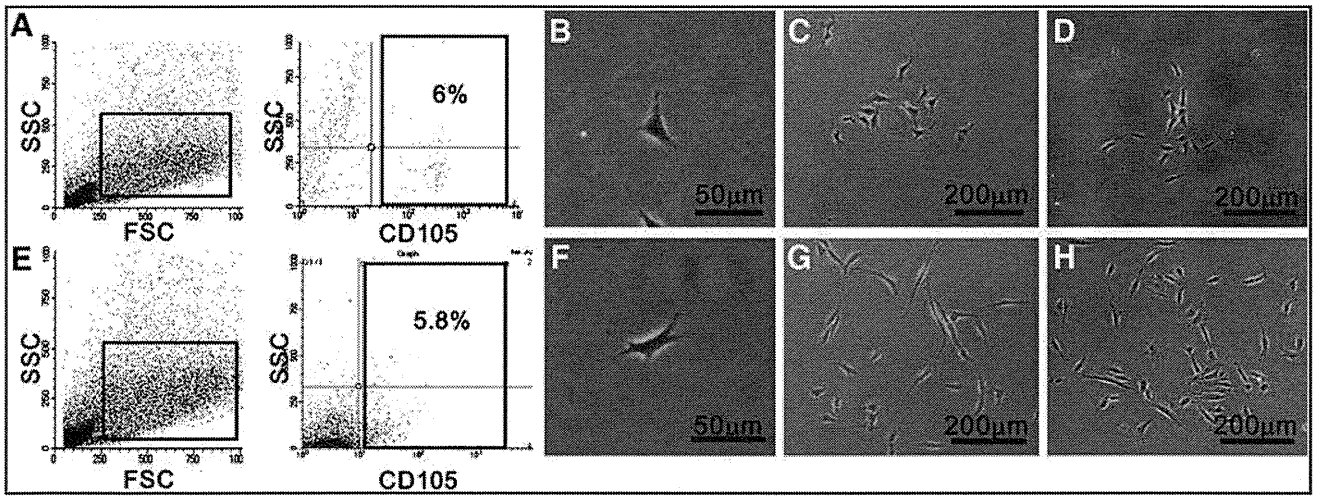

FIG. 1. Isolation of CD105$^+$ cells from adult canine dental pulp and adipose tissue. **(A)** The two panels show flow cytometry profiles of forward scatter (FSC) and side scatter (SSC) (left), and CD105 and SSC expression (right) on the dental pulp tissue. CD105$^+$ cells represented 6% of the total. **(B)** Primary pulp CD105$^+$ cell culture on day 3. **(C)** Primary pulp CD105$^+$ cell culture on day 10. **(D)** Primary total pulp cells on day 10. **(E)** The two panels show flow cytometry profiles of FSC and SSC (left), and CD105 and SSC expression (right) on the adipose tissue. CD105$^+$ cells represented 5.8% of the total. **(F)** Primary adipose CD105$^+$ cell culture on day 3. **(G)** Primary adipose CD105$^+$ cell culture on day 10. **(H)** Primary total adipose cells on day 10. The experiments were repeated nine times, and one represented experiment is presented. Color images available online at www.liebertonline.com/tea

(5 μm in thickness) were morphologically examined after staining with hematoxylin and eosin (HE).

All animal experiments were conducted using the strict guidelines of the Animal Protocol Committees and DNA Safety Programs both in National Center for Geriatrics and Gerontology and Aichigakuin University.

For vascular staining, 5-μm-thick paraffin sections stained with Fluorescein Griffonia (Bandeiraea) Simplicifolia Lectin 1/fluorescein-galanthus nivalis (snowdrop) lectin (20 μg/mL; Vector laboratories) for 15 min a fluorescence microscope BIOREVO, BZ-9000 (KEYENCE) were used.

For whole mount staining of vascular structure, the regenerated tissue and normal pulp tissue were dissected from teeth on day 14 and fixed in 4% paraformaldehyde for 45 min. The tissue was treated with 0.3% Triton X in phosphate-buffered saline, blocked, and stained with isolectin GS-IB4 from Griffonia simplicifolia, Alexa Fluor 488 conjugate (1:500) for 12 h at 4°C overnight. Neovascularization and engraftment of the transplanted cells into the root canal was examined by two-photon microscopy using FV1000MPE (Olympus) instrument. Three-dimensional structures were reconstructed by FV10-ASW software.

For neuronal staining, 5-μm-thick paraffin sections were incubated for 15 min with 0.3% Triton X-100 (Sigma Chemical). After incubation with 2.0% normal goat serum to block non-specific binding, they were incubated with goat anti-human PGP9.5 (Ultra Clone) (1:10000) at 4°C overnight. After three washes in phosphate-buffered saline, bound antibodies were reacted with biotinylated goat anti-rabbit IgG secondary antibody (Vector) (1:200) for 1 h at room temperature. The sections were also developed with the ABC reagent (Vector Laboratories), using the DAB chromogen for 10 min.

Relative amounts of regenerative pulp tissue 14 days after transplantation were examined in each sample by capturing video images of the histological preparations on the binocular microscopy (Leica, M 205 FA). Three sections at 150-μm intervals for each tooth from a total of 5 teeth each transplanted with pulp CD105$^+$ cells with SDF-1, adipose CD105$^+$ cells with SDF-1, total pulp cells with SDF-1, pulp CD105$^+$ cells only, SDF-1 only, and collagen TE scaffold only were examined. On-screen image outlines of newly regenerated pulp tissue and newly formed dentin were traced, and the surface area of these outlines in the root canal was determined by using Leica Application Suite software. The ratio of the regenerated area to the root canal area was calculated in three sections of each tooth, and the mean value was determined.

In vivo gene expression of odontoblastic differentiation markers, *dentin sialophosphoprotein* (*Dspp*) and *enamelysin*, in the cells lining along the root canal surface was examined by

TABLE 1. FLOW CYTOMETRIC ANALYSIS OF CELL-SURFACE MARKERS ON PULP AND ADIPOSE-DERIVED CD105$^+$ CELLS AND TOTAL PULP CELLS AT THE THIRD PASSAGE OF CULTURE

	Pulp CD105$^+$ cells	*Adipose CD105$^+$ cells*	*Total pulp cells*
CD24	1.8%	1.7%	0.3%
CD29	95.9%	90.5%	99.2%
CD31	0%	0%	0%
CD33	3.7%	0%	0.2%
CD34	45.5%	0.1%	47.1%
CD44	96.2%	92.3%	99.9%
CD73	97.2%	0.8%	22.3%
CD90	98.1%	95.6%	97.5%
CD105	98.5%	74.0%	4.6%
CD146	0.8%	0.2%	0.9%
CD150	2.3%	0.2%	0.9%
MHC class I	36.0%	80.0%	73.8%
MHC class II	0.4%	0%	0.4%
CXCR4	12.2%	5.9%	5.3%

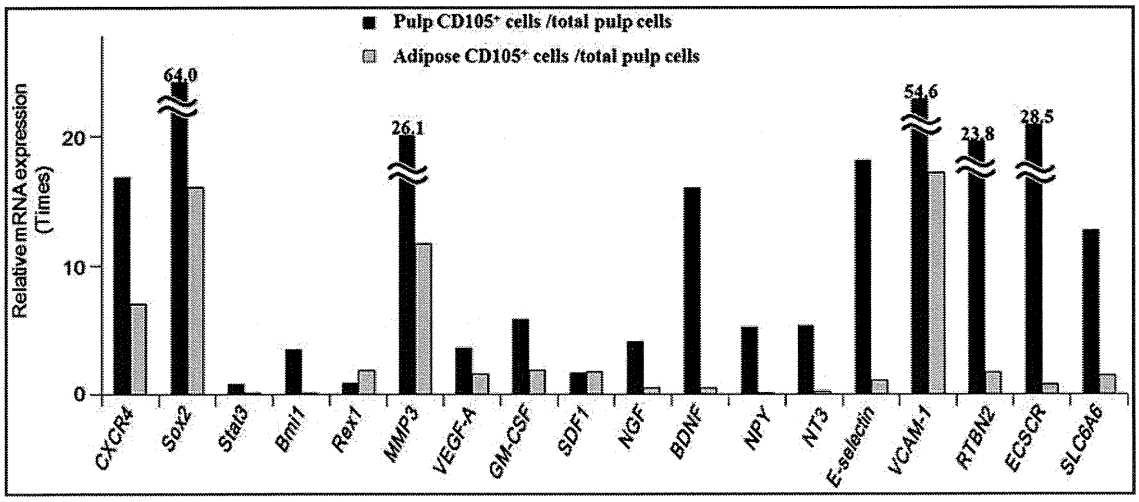

FIG. 2. Relative mRNA expression of cytokines of vasculogenesis and neurogenesis by real-time reverse transcription-polymerase chain reaction in pulp and adipose-derived CD105$^+$ cells. The experiments were repeated four times, and one represented experiment is presented.

in situ hybridization in 5 μm-paraffin sections 90 days after transplantation of pulp CD105$^+$ cells with SDF-1. Canine cDNA of *Dspp* (183 bp) and *enamelysin* (195 bp) linearized with *Nco*I and *Spe*I, respectively, were used as anti-sense probes. The probes were constructed out of the plasmids after subcloning the PCR products using the same primers as those designed for real-time RT-PCR (Supplementary Table S1). The DIG signals were detected by TSA system (PerkinElmer).

Two-dimensional electrophoretic analyses and gene expression analyses

For two-dimensional electrophoretic analysis, the regenerated pulp-like tissue on day 28, normal pulp, and periodontal ligament were homogenized in lysis buffer (6 M urea, 1.97 M thiourea, 2% [w/v] 3-[(3-cholamidopropyl) dimethylammonio] propanesulfonate, 64.8 mM dithiothreitol [DTT], 2% [v/v] Pharmalyte) and sonicated. The supernatant was collected after being centrifuged at 15,000 rpm for 15 min at 4°C, and applied to two-dimensional electrophoresis. Isoelectric focusing (IEF) was carried out using CoolPhoreSter 2-DE systems. IPG strips (Immobiline DryStrips, pH 4–7, 18 cm; GE) were used according to the manufacturer's instructions. IPG strips were rehydrated with rehydration solution (6 M urea, 1.97 M thiourea, 2% [v/v] TritonX-100, 13 mM DTT, 2% [v/v] Pharmalyte, 2.5 mM acetic acid, 0.0025% bromophenol blue [BPB]) overnight at 20°C. IEF was performed following a step-wise voltage incremental manner: 500 V for 2 h, 700–3000 V for 1 h, and 3500 V for 24 h. After IEF, IPG strips were incubated in an equilibration buffer (6 M urea, 32.4 mM DTT, 5 mM Tris-HCl, pH 6.8, 2% [w/v] sodium dodecyl sulfate [SDS], 0.0025% BPB, 30% [v/v] Glycerol) for 30 min. IPG strips were further equilibrated in 5 mM Tris-HCl, pH 6.8, 2% (w/v) SDS, 0.0025% BPB, 30% (v/v) Glycerol, and 243 mM iodoacetamid for 20 min. Separation in the second dimension was carried out in 12.5% SDS-PAGE gels (20 cm × 20 cm) at a constant current of 25 mA/gel for 15 min and 30 mA/gel thereafter. The gels were stained with Flamingo Fluorescent Gel Stain (Bio-Rad Laboratories) and scanned (FluoroPhorester 3000; Anatech). The gel images were analyzed and compared with each other by using Progenesis (Nonlinear Dynamics).

Real-time RT-PCR amplifications were performed as previously described using markers for periodontal ligament, canine *axin2*, *periostin*, and *asporin*/periodontal ligament-associated protein 1 (*PLAP-1*). *Collagen αI(I)*, *syndecan3*, and *tenascin C* were also used for comparison of regenerated tissue with normal pulp and periodontal ligament (Supplementary Table S1).

For microarray analysis, biotinylated cRNA were prepared from 250 ng of total RNA according to the standard Affymetrix protocol (Affymetrix Japan K.K.). After fragmentation, 10 μg of cRNA were hybridized for 16 h at 45°C on GeneChip Canine Genome 2.0 Array (Affymetrix) containing ~43,000 annotated sequences. GeneChips were washed and stained in the Affymetrix Fluidics Station 450, and were scanned using the Affymetrix GCS3000 scanner. The data were analyzed with Microarray Suite version 5.0 (MAS 5.0) using Affymetrix default analysis settings and global scaling as normalization method. The trimmed mean target intensity of each array was set to 500. Chips were ordered into hierarchical clusters using the Pearson centered algorithm as the distance measure, and the Average algorithm as the linkage method.

Statistical analyses

Data are reported as means ± standard deviation. *p*-Values were calculated by using the unpaired Student's *t*-test. The number of replicates in each experiment is indicated in the figure legends.

Results

Isolation and characterization of CD105$^+$ cells from pulp and adipose tissue

Flow cytometric isolation of the CD105$^+$ cells from canine adult total pulp cells (Fig. 1D) was performed using antibodies against CD105. CD105$^+$ cells isolated from total adipose cells (Fig. 1H) of the same dog and unfractionated total pulp cells were used as controls. The pulp and adipose